

Patterns of Alluviation in Mixed Bedrock-Alluvial Channels: 2. Controls on the Formation of Alluvial Patches

Jongseok Cho¹ and Peter A. Nelson¹

¹Colorado State University

June 11, 2023

Abstract

Understanding the development and spatial distribution of alluvial patches in mixed bedrock-alluvial rivers is necessary to predict the mechanisms of the interactions between sediment transport, alluvial cover, and bedrock erosion. This study aims to analyze patterns of bedrock alluviation using a 2D morphodynamic model, and to use the model results to better understand the mechanisms responsible for alluvial patterns observed experimentally. A series of simulations are conducted to explore how alluvial patterns in mixed bedrock-alluvial channels form and evolve for different channel slopes and antecedent sediment layer thicknesses. In initially bare bedrock low-slope channels, the model predicts a linear relationship between sediment cover and sediment supply because areas of subcritical flow enable sediment deposition, while in steep-slope channels the flow remains fully supercritical and the model predicts so-called runaway alluviation. For channels initially covered with sediment, the model predicts a slope-dependent sediment supply threshold above which a linear relationship between bedrock exposure and sediment supply develops, and below which the bedrock becomes fully exposed. For a given sediment supply, the fraction of bedrock exposure and average alluvial thickness converge toward the equilibrium value regardless of the initial cover thickness so long as it exceeds a minimum threshold. Steep channels are able to maintain a continuous strip of sediment under sub-capacity sediment supply conditions by achieving a balance between increased form drag as bedforms develop and reduced surface roughness as the portion of alluvial cover decreases. In lower-slope channels, alluvial patches are distributed sporadically in regions of the subcritical flow.

15 **Abstract**

16 Understanding the development and spatial distribution of alluvial patches in mixed bedrock-
17 alluvial rivers is necessary to predict the mechanisms of the interactions between sediment
18 transport, alluvial cover, and bedrock erosion. This study aims to analyze patterns of bedrock
19 alluviation using a 2D morphodynamic model, and to use the model results to better understand
20 the mechanisms responsible for alluvial patterns observed experimentally. A series of
21 simulations are conducted to explore how alluvial patterns in mixed bedrock-alluvial channels
22 form and evolve for different channel slopes and antecedent sediment layer thicknesses. In
23 initially bare bedrock low-slope channels, the model predicts a linear relationship between
24 sediment cover and sediment supply because areas of subcritical flow enable sediment
25 deposition, while in steep-slope channels the flow remains fully supercritical and the model
26 predicts so-called runaway alluviation. For channels initially covered with sediment, the model
27 predicts a slope-dependent sediment supply threshold above which a linear relationship between
28 bedrock exposure and sediment supply develops, and below which the bedrock becomes fully
29 exposed. For a given sediment supply, the fraction of bedrock exposure and average alluvial
30 thickness converge toward the equilibrium value regardless of the initial cover thickness so long
31 as it exceeds a minimum threshold. Steep channels are able to maintain a continuous strip of
32 sediment under sub-capacity sediment supply conditions by achieving a balance between
33 increased form drag as bedforms develop and reduced surface roughness as the portion of
34 alluvial cover decreases. In lower-slope channels, alluvial patches are distributed sporadically in
35 regions of the subcritical flow.

36 **Plain Language Summary**

37 Bedrock rivers may have patches of alluvial sediment that covers some or all of the underlying
38 bedrock. The amount of this sediment cover can change dynamically over time depending on the
39 flow, upstream sediment supply, channel morphology, and antecedent sediment conditions. Here,
40 we use a numerical model to simulate flow and sediment transport so that we may better
41 understand what controls sediment cover in mixed bedrock-alluvial rivers. We use the model to
42 simulate channels of varying slopes, sediment supplies, and initial sediment cover, and we
43 analyze the model's output to gain insight on how alluvial patches form and what controls their
44 extent and dynamics. Our numerical model results produce phenomena that have been observed
45 in physical experiments, and they show that the channel slope and initial sediment thickness
46 plays an important role in determining whether and how much sediment can be deposited. Our
47 results also show that flow transitions provide critical locations where sediment deposits can start
48 to form. Persistent sediment cover in bedrock channels can develop when a delicate equilibrium
49 is reached between sediment roughness and the flow field.

50 **1 Introduction**

51 Bedrock channels are characterized by occasional or continuous exposures of
52 nonalluviated bedrock, which is a consequence of these channels receiving a sediment supply
53 that is less than their transport capacity. A wide variety of models for drainage network evolution
54 distinguish between bedrock and alluvial reaches (Howard, 1980; Howard et al., 1994; Howard
55 & Kerby, 1983; Montgomery et al., 1996) by using channel slope and discharge to express
56 channel transport capacity. Field investigations (Lamb et al., 2008; Massong & Montgomery,
57 2000; Montgomery et al., 1996; Montgomery & Buffington, 1997) demonstrate that bedrock
58 channels occur at slopes greater than a critical value ($S > S_c$), and alluvial channels form at a
59 slope less than the critical value ($S \leq S_c$).

60 The spatial distribution of alluvial cover in mixed bedrock-alluvial channels has
61 importance for determining rates and patterns of bedrock erosion, hydrodynamics, and aquatic
62 habitat. Mechanistic models of bedrock erosion incorporate the erosional mechanism of saltating
63 bedload particles impacting and eroding bedrock (e.g., Demeter et al., 2005; Hartshorn et al.,
64 2002; Sklar & Dietrich, 1998, 2001, 2004; Zhang et al., 2015), implicitly introducing
65 dependence on sediment supply and bedrock exposure into the calculation of erosion rates.
66 Competition between the tools and cover effects controls the spatial distribution of the bedrock
67 channel erosion, resulting in lateral and vertical channel erosion and meandering (Finnegan et al.,
68 2007; Lamb et al., 2015; Turowski et al., 2007; Turowski, Hovius, Meng-Long, et al., 2008;
69 Turowski, Hovius, Wilson, et al., 2008). The cover effect is typically demonstrated by linear or
70 exponential relations of fractional bedrock exposure as a function of sediment supply to transport
71 capacity ratio (Sklar & Dietrich, 1998, 2004; Turowski et al., 2007). Additionally, sediment
72 supply and alluvial cover impact the maintenance and distribution of aquatic habitat and attached
73 micro-organisms (Buffington et al., 2004; Detert & Parker, 2010; Huston & Fox, 2015, 2016;
74 Kuhnle et al., 2013; Lisle & Hilton, 1992; Lisle & Lewis, 1992; Madej, 2001).

75 Alluvial patterns in bedrock channels are controlled by spatial and temporal variations in
76 sediment flux, transport capacity, and bed topography. These channels can exhibit alluvial
77 patterns ranging from continuous and concentrated longitudinal strips of sediment to spatially
78 discontinuous patches of sediment. Experiments in mixed bedrock-alluvial channels have
79 observed spatially concentrated sediment cover and storage in low parts of the underlying
80 bedrock topography (Finnegan et al., 2007; Johnson & Whipple, 2007), indicating that
81 topographic roughness induces changes in local flow properties and threshold of sediment
82 motion. Inoue et al. (2014) observed inconsistent development of alluvial cover in the inner

83 channel through their field experiments. Hodge and Hoey's (2016a, 2016b) experiments show
84 that velocity is an important control on sediment deposition, as they did not observe sediment
85 cover at low areas of the bed where the flow velocity remained high. The results from several
86 experimental studies (Chatanantavet & Parker, 2008; Johnson & Whipple, 2010; Sklar &
87 Dietrich, 2004; Turowski et al., 2007) suggest a few major factors control grain entrainment and
88 bedrock exposure, such as sediment supply rate, channel slope, material size, and bed roughness.

89 A set of flume experiments (Chatanantavet & Parker, 2008) using different channel bed
90 slopes has shown that for lower slopes ($S < 0.0115$) bedrock exposure decreased more or less
91 linearly with increasing the ratio of sediment supply rate to capacity transport rate. However, for
92 sufficiently higher slopes ($S \geq 0.0115$), the bedrock remained fully exposed when the ratio of
93 sediment supply to transport capacity is less than a critical value, while a linear relationship
94 between the degree of bedrock exposure and sediment supply rate to transport capacity ratio
95 prevailed when the sediment supply exceeds transport capacity. These experiments also
96 documented a slope-dependent “runaway alluviation,” where for initially bare-bedrock
97 conditions, low-slope channels develop linearly increasing sediment cover with increasing
98 sediment supply, while high-slope channels remain completely exposed until sediment supply
99 exceeds the transport capacity, beyond which the channel becomes fully alluviated.

100 Chatanantavet and Parker (2008) suggested this may be a result of slope-dependent grain
101 interactions; later experiments by Mishra and Inoue (2020) indicated that runaway alluviation
102 occurred when the bedrock roughness was lower than the sediment roughness, but the gradual
103 alluvial cover could develop when the bedrock roughness was higher than that of the sediment. A
104 full explanation of the slope-dependent behavior of sediment dynamics in mixed bedrock-
105 alluvial channels is still needed.

106 Morphodynamic models have struggled to replicate the types of observations made in
107 mixed bedrock-alluvial experiments. Promising results have been presented by Hodge and Hoey
108 (2012), who developed a cellular automaton (CA) model where the probability of entrainment of
109 individual grains was specified for bedrock or alluvial areas. Their model found relationships
110 between bedrock exposure and the ratio of sediment supply to transport capacity (q_s/q_c) similar to
111 those observed by Chatanantavet and Parker (2008), but in contrast to the experimental
112 observations, the majority of their CA model runs predicted that the presence or absence of
113 sediment cover on the bed at the beginning of the run did not affect the steady state sediment
114 cover. Additionally, the entrainment probabilities needed to change from run to run for their
115 results to achieve the diversity of findings Chatanantavet and Parker (2008) reported. While CA
116 models like this provide interesting insight on the potential importance of grain dynamics for
117 alluvial patterns in bedrock-alluvial channels, the absence of a flow model makes connecting
118 probabilities of sediment entrainment and deposition to physical mechanisms of sediment
119 transport and alluviation challenging.

120 Because of the complexity inherent in the roughness relationship incorporated to the flow
121 resistance and sediment transport, evaluating the relative influence of different roughness
122 mechanisms for channel evolution is currently a challenging problem. The patterns of sediment
123 cover over the bedrock bed affect the spatial distribution of local roughness, flow rate, and
124 sediment transport. Here we use a new morphodynamic model to reproduce many of the
125 phenomena that have been observed in mixed bedrock-alluvial channels, and we use the model
126 predictions to untangle the mechanisms responsible for the range of dynamic sediment behavior
127 in these environments. In particular, we use the model to investigate the following questions: 1)
128 what explains the apparent slope dependence for runaway alluviation? 2) How can mixed

129 bedrock-alluvial channels maintain alluvial cover when the sediment supply is less than the
130 transport capacity? 3) How do initial conditions of sediment cover affect the temporal
131 development of alluvial cover, and the overall relationship between bedrock exposure and
132 sediment supply? Our results reveal the important interactions between dynamic channel
133 roughness, flow patterns, sediment transport rates, bedform development, and alluvial cover.

134 **2 Methods**

135 2.1 Morphodynamic model

136 We have developed a two-dimensional numerical morphodynamic model for mixed
137 bedrock-alluvial channels. The model is fully described in Cho and Nelson (submitted), and we
138 summarize the key aspects of the model here. The model consists of three major components: (1)
139 the 2D shallow water equations (SWE) in the depth-averaged form are applied to solve the
140 hydrodynamical component, (2) a sediment transport model calculates bedload transport rates
141 associated with the hydrodynamic variables and topographic variation, and (3) the modified
142 Exner equation, which computes changes in alluvial concentration or thickness due to sediment
143 transport divergence. The novel aspects of this model, compared to previous models applied to
144 mixed bedrock-alluvial morphodynamics, are 1) the Exner equation of sediment continuity
145 accounts for the volume of bedload in transport and the fraction of bed covered in sediment, 2) a
146 composite alluvial and bedrock roughness is used in the flow calculation, 3) the friction for
147 sediment transport is modified to account for the effects of bedforms, and 4) the numerical
148 scheme is robust and capable of handling Froude transitions and capturing shocks. We
149 summarize the key components of the model below.

150 A key assumption in most numerical models combining water flow, sediment transport,
151 and morphological evolution is that the response time of bed evolution is relatively long
152 compared to the timescales of relevance to the flow of water (McLean et al., 1994; Nelson et al.,
153 2003; Tubino et al., 1999). This allows a decoupling between the water flow computation and the
154 sediment equation by assuming a quasi-steady approximation of morphodynamic process that the
155 bed level does not change rapidly during an infinitesimal time interval while the flow field
156 adapts instantaneously. Thus, the decoupled model practically solves for the flow field and
157 topographic evolution using an iterative procedure.

158 Mixed bedrock-alluvial channels exhibit complex roughness feedbacks due to differential
159 roughness of alluvium and bedrock surfaces, the development of bedforms and associated form
160 drag, as well as bed shear stress taken up by sediment transport itself. To account for this, our
161 model uses a composite roughness partitioned into surface roughness of alluvial and bedrock
162 bed, sediment transport roughness, and form drag. The ripple factor is applied to the shear stress
163 to remove the form drag of the bedforms assuming the remaining part is responsible for sediment
164 transport.

165 Water depth and flux are calculated using the Harten-Lax-van Leer-Contract (HLLC)
166 scheme with the weighted average flux (WAF) method (Toro, 1992a, 1992b) and an explicit
167 application of the central difference of the viscous and friction terms at each computational cell
168 center in a 2D domain. Because of the local and global change in flow resistance associated with
169 different substrate roughness between the bedrock and bed material and bedform evolution, a
170 treatment of transcritical flow is necessary. The flow resistance consists of skin friction, form
171 drag, and bedload transport roughness. A linear fractional cover model representing the relation
172 between the alluvial bed and bare bedrock bed, the volume of local bed material per volume of a

173 monolayer of sediment grains, is used to calculate local skin friction. The form drag effect is
 174 determined using the local bed slope and topographic variation averaged over the area of interest.
 175 Additionally, the bedload layer thickness is added to the total roughness where the sediment
 176 transport occurs. The explicit calculation of each of these components of roughness is critical to
 177 be able to replicate observations of persistent sediment cover in mixed bedrock-alluvial channels
 178 (Cho and Nelson, submitted).

179 The bed morphology is updated using the modified Exner equation for sediment
 180 continuity (Inoue et al., 2014, 2016; Luu et al., 2004). The sediment transport capacity on the
 181 alluvial bed is estimated from Wong et al. (2007). A correction of the bedload transport rate on
 182 the pure bedrock bed is necessary considering a relatively small volume of bedload transport:

$$183 \quad q_b = \begin{cases} \frac{V_b}{V_{bc}} q_{bc} & \text{for } 0 \leq V_b < V_{bc} \\ q_{bc} & \text{for } V_{bc} \leq V_b \end{cases} \quad (1)$$

184 where q_b is the bedload transport rate per unit width, q_{bc} is the bedload transport capacity per
 185 unit width, V_b is the volume of sediment per unit area in the bedload layer, and V_{bc} is the
 186 saturation volume per unit area in the bedload layer. When the bed is completely bare, only the
 187 volume of sediment in the bedload layer is brought into bedload transport without resting on the
 188 bed, referred to as the throughput bedload. When the volume of the bedload layer exceeds the
 189 saturation value, sediment starts to deposit on the bed and the linear cover fraction model is
 190 utilized to determine whether the bed is in the state of partial or complete cover:

$$191 \quad \eta_a = \begin{cases} \frac{V_{ba} - V_{bc}}{1 - \lambda} & \text{for } V_{bc} \leq V_{ba} \\ 0 & \text{for } 0 \leq V_{ba} < V_{bc} \end{cases} \quad (2)$$

192 where η_a is the alluvial layer thickness, V_{ba} is the total volume of sediment per unit area in
 193 alluvial bedload layers, λ is the porosity, and

$$194 \quad V_b = \begin{cases} V_{bc} & \text{for } V_{bc} \leq V_{ba} \\ V_{ba} & \text{for } 0 \leq V_{ba} < V_{bc} \end{cases} \quad (3)$$

195 where $V_{bc} = q_{bc}/u_s$ and u_s is the saltation velocity.

196 The skin friction is used for the calculation of dimensionless shear stress to account for
 197 the fact that only the near-bed grain roughness is responsible for the sediment transport, using a
 198 correction referred as to the ripple factor (Ribberink, 1987; Vermeer, 1986). The dimensionless
 199 shear stress (Struiksma, 1985; Talmon et al., 1995) and critical Shields number (Calantoni, 2002;
 200 Duan & Julien, 2005; Soulsby, 1997) are corrected for spatially varying bed topography in the
 201 direction of flow.

202 The critical Shields parameter calculated as a function of the ratio of the bedrock
 203 hydraulic roughness to the grain size (Inoue et al., 2014; Johnson, 2014; Mishra & Inoue, 2020)
 204 is adopted instead of constant value for bedrock and alluvial surfaces. We use a modified
 205 dimensionless critical shear stress model to simulate bed evolution in different channel slopes:

$$206 \quad \tau_c^* = \alpha_c (k_0/d)^{0.6} \quad (4)$$

207 where α_c is the correction factor for different channel slopes, k_0 is the hydraulic roughness
 208 height, and d is the grain size.

209 2.2 Simulation conditions

210 We conducted a set of numerical experiments to explore how channel slope, initial
 211 sediment cover thickness, and sediment supply impact the evolution of patterns of alluvial cover

212 in mixed bedrock-alluvial channels. The simulations were designed to complement the
213 experiments of Chatanantavet and Parker (2008) and provide mechanistic insight into controls on
214 alluvial patterns in bedrock channels. Table 1 summarizes the initial flow and sediment condition
215 used in each experiment based on the flume experiments conducted by Chatanantavet and Parker
216 (2008). The computational channel is straight and longer than the experimental channel to avoid
217 possible problems regarding bedform development sensitive to boundary disturbances. All
218 simulations impose constant water and sediment supply, uniform sediment size, and non-erodible
219 bedrock to exclude potential disturbances to bed topography created by unsteady conditions. The
220 computations are stopped when near equilibrium conditions of bed topography are achieved, in
221 which the average sediment cover thickness and the fraction of bedrock cover vary around stable
222 values.

223 All simulations are performed in a rectangular bedrock channel having a length of 20 m
224 and a width of 0.9 m. Small topographic variations with a standard deviation of 2.2 mm and
225 peak-to-peak bed elevation of 9 mm are applied to the bedrock bed. First, two sets of simulations
226 are performed: (1) with some initial cover thickness with different channel slopes (Runs 2-A5
227 and 2-B5) and (2) without antecedent sediment cover (Runs 2-Ax, 2-Bx, and 2-Dx) to explore
228 the effect of channel slopes. Second, a set of Run 2-B is conducted with the $q_s/q_c = 0.6$ and
229 various initial sediment cover thicknesses of 1, 4, and 6 cm. Two types of uniform grains, fine 2
230 mm and coarse 7 mm gravels, are employed in the experiments with a mild slope channel (
231 $S \leq 0.0115$) and with a steep slope channel ($S = 0.02$), respectively.

Table 1. Summary of Flow, Sediment Transport, and Topographic Conditions^a

	mm		%	cm	l/s	g/s	g/s		mm	cm	cm/s	
RUN	k_b	α_c	S	Z_{bi}	Q_w	Q_c	Q_s	Q_s/Q_c	d	H	U	F_e
2-A1	0.4	0.03	1.15	1.5	24	25	5	0.2	2	4.3	62	0.78
2-A2	0.4	0.03	1.15	1.5	24	25	10	0.4	2	4.3	62	0.6
2-A3	0.4	0.03	1.15	1.5	24	25	15	0.6	2	4.3	62	0.41
2-A4	0.4	0.03	1.15	1.5	24	25	20	0.8	2	4.3	62	0.27
2-A5	0.4	0.03	1.15	1.5	24	25	25	1.0	2	4.5	59	0
2-B1	4	0.05	2	2	55	110	44	0.4	7	5	122	1
2-B2	4	0.05	2	2	55	110	66	0.6	7	5.5	111	0.4
2-B3	4	0.05	2	2	55	110	88	0.8	7	5.5	111	0.25
2-B4	4	0.05	2	2	55	110	110	1.0	7	6	102	0
2-B2-a	4	0.05	2	1	55	110	66	0.6	7	5	122	1
2-B2-b	4	0.05	2	4	55	110	66	0.6	7	6	102	0.4
2-B2-c	4	0.05	2	6	55	110	66	0.6	7	6	102	0.4
2-Ax	0.4	0.03	1.15	0	24	150	150	1.0	2	2.9	92	0
2-Bx	4	0.05	2	0	55	350	350	1.0	7	5	122	0
2-Dx-a	0.2	0.08	0.3	0	55	8	2	0.25	2	7.5	81	0.7
2-Dx-b	0.2	0.08	0.3	0	55	8	4	0.5	2	7.5	81	0.6
2-Dx-c	0.2	0.08	0.3	0	55	8	6	0.75	2	7.5	81	0.52
2-Dx-d	0.2	0.08	0.3	0	55	8	8	1.0	2	7.5	81	0

^aThe run names correspond to Chatanantavet and Parker's (2008) experimental conditions. k_b denotes bedrock roughness height, α_c denotes Shields number correction coefficient, S denotes channel slope, Z_{bi} denotes initial sediment cover thickness, Q_w denotes water discharge, Q_c denotes sediment transport capacity, Q_s denotes sediment supply rate, q_s/q_c denotes the ratio of sediment supply to transport capacity, d denotes grain size, H denotes flow depth, U denotes flow velocity, and F_e denotes the fraction of bedrock exposure, respectively.

232 The bedrock and grain roughness heights are back-calculated from the logarithmic law
233 depending on the channel slope and corresponding hydraulic conditions. The spatially varying
234 friction coefficient is then calculated as a function of the flow depth and composite roughness,
235 which depends upon the local status of fraction cover, bedform dimension, and bedload transport

236 rate. The critical Shields parameters for each channel slope are back-calculated by equating the
237 sediment transport capacity from our numerical simulations and experimental runs of
238 Chatanantavet and Parker (2008) conducted in bedrock channels, and adjustment to the
239 correction coefficient α_c is employed.

240 In each simulation, the sediment supply q_s was specified as a target fraction of the
241 transport capacity q_c . To determine q_c , we conducted simulations for each run, assuming that
242 the initial bed is nearly flat for either with initial sediment cover (Runs 2-A and 2-B) or bare
243 bedrock surface (Runs 2-Ax, 2-Bx, and 2-Dx) without the presence of bedforms. The bedrock
244 transport capacity is the lowest rate of sediment input per unit width fed into the initially bare
245 bedrock bed that results in equilibrium conditions where the bed is completely covered ($F_e = 0$).
246 The alluvial transport capacity is the channel averaged sediment transport rate in the alluvial
247 channel.

248 **3 Results**

249 3.1 Simulations with no initial alluvial cover

250 Runs 2-Ax, 2-Bx, and 2-Dx all commenced with a bare bedrock bed, and are used to
251 investigate how channel slope affects sudden vs. gradual alluviation as sediment supply
252 increases. The lowest-slope simulations ($S = 0.003$) of Run 2-Dx exhibited a gradual decrease in
253 bedrock exposure at increasing sediment supplies. An example of bed evolution for these runs is
254 shown in Figure 1 for Run 2-Dx-a, for which bedrock surface roughness was 0.2 mm and the
255 ratio of sediment supply to transport capacity was $q_s/q_c = 0.25$. The time evolution of alluvial
256 cover illustrates that the sediment grains initially deposit in the lower topography areas, and
257 sediment patches gradually grow thicker and expand in the upstream direction.

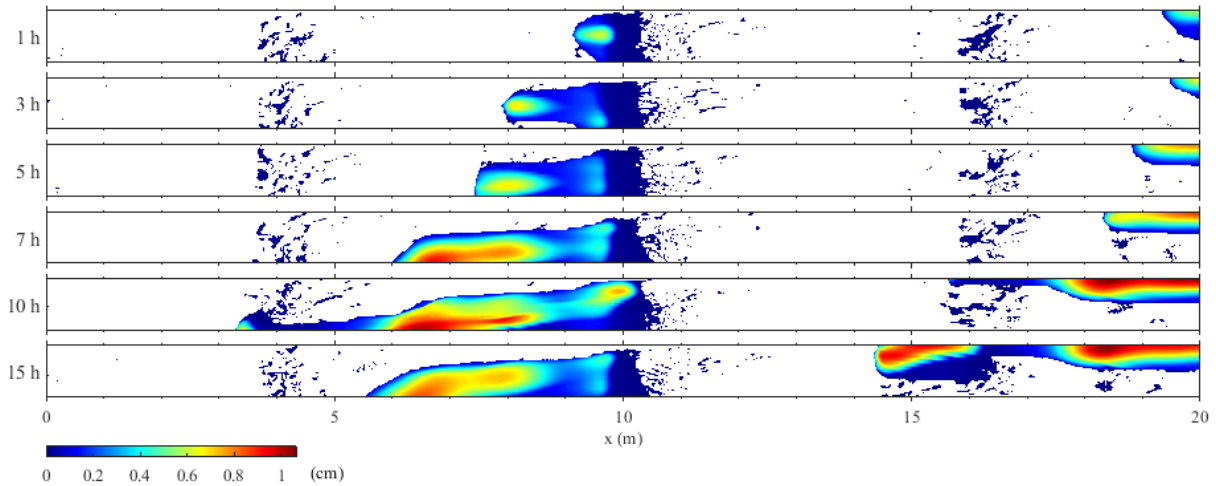


Figure 2. Simulated bed evolution of Run 2-Dx-a, which began with a bare bedrock bed and sediment supplied at $q_s/q_c = 0.25$. Colorbar shows the thickness of the sediment cover, and white areas correspond to the exposed bedrock surface.

258 Figure 2 shows the final state of alluviation for all of the low-slope 2-Dx runs. As

259 sediment supply (i.e., q_s/q_c) increases, the alluviated patches grow in size and the overall

260 fraction of exposed bedrock (F_e) decreases.

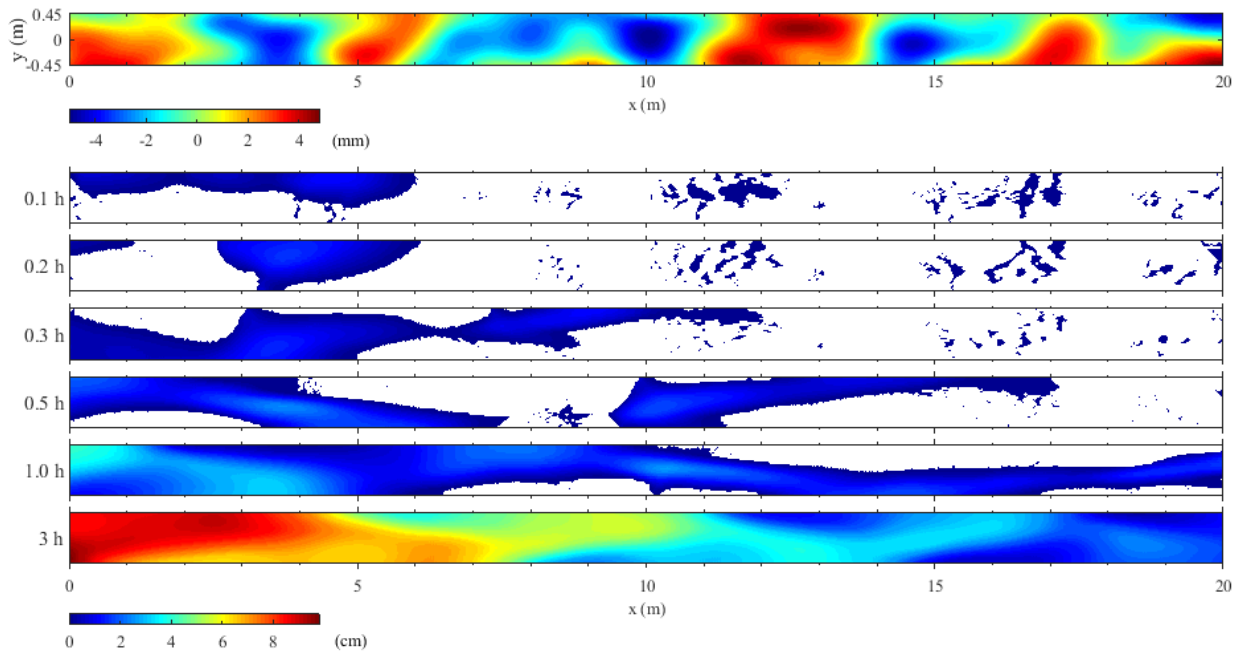


Figure 1. Plan view of bedrock topography (top). Colorbar scale indicates the detrended bed elevation. Simulated bed evolution of Run 2-Bx with $q_s/q_c = 1$ (bottom). Colorbar shows the thickness of the sediment cover, and white areas correspond to the exposed bedrock surface.

261 Figure 3 shows the time evolution of alluvial patch formation for simulation Run 2-Bx,
 262 which commenced from the bare bedrock bed in a channel with a higher slope of 0.02. For this
 263 run, bedrock roughness was 4 mm and sediment was supplied at the channel's transport capacity
 264 ($q_s/q_c = 1$). The sediment tends to deposit on the stoss side of the bedrock mounds where low
 265 flow velocity results in low Froude number, shear stress, and sediment transport capacity. The
 266 sediment forms small patches that grow in size as they move downstream. The migrating alluvial
 267 patches bypass the high bedrock areas by moving through the topographic lows. A sediment strip
 268 develops and shifts from one side of the channel to the other, and the entire channel bed is
 269 eventually covered with sediment. Complete alluviation of the bedrock bed begins from the
 270 upstream end of the channel, and alternate-bar-like patterns form as sediment moves across the
 271 channel.

272 Unlike the lower-slope runs of 2-Dx, simulations for 2-Ax ($S = 0.0115$) and 2-Bx ($S = 0.02$)
 273 were not able to achieve persistent alluvial cover for sediment supplies less than the
 274 transport capacity. Figure 4a demonstrates how the fraction of exposed bedrock surface varies
 275 with the sediment supply to transport capacity ratio in the initially bare bedrock channel. In
 276 steep-slope channels ($S \geq 0.0115$) without preexisting sediment, the bedrock bed remains fully

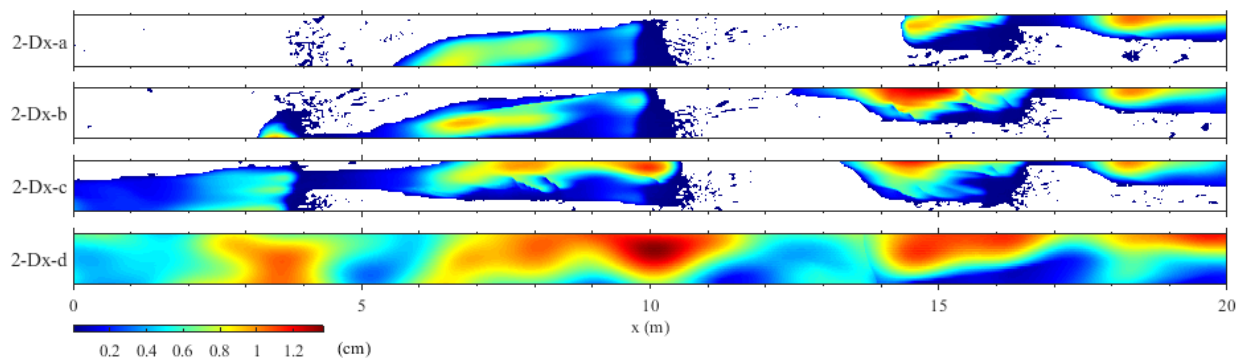


Figure 3. Plan view of Runs 2-Dx at equilibrium. The sediment is supplied at $q_s/q_c = 0.25, 0.5, 0.75,$ and 1.0 , from top to bottom. Colorbar shows the thickness of the sediment cover, and white areas correspond to the exposed bedrock surface.

277 exposed while the sediment supply rate is less than the channel sediment transport capacity.
 278 When the sediment supply momentarily exceeds the threshold value, the entire bedrock bed is
 279 completely covered by sediment, so-called “runaway alluviation”. In contrast, in the lower slope
 280 channel ($S = 0.003$, Run 2-Dx), the fractional bedrock exposure declines with increasing
 281 sediment supply in a more or less linear fashion at below-capacity sediment supply. These results
 282 are qualitatively and quantitatively similar to the observations of Chatanantavet and Parker
 283 (2008), whose experimental results are plotted alongside ours on the same figure (Figure 4).

284 3.2 Simulations with initial alluvial cover and varying slope

285 Figure 4b compares the model-predicted and experimentally observed relationships
 286 between bedrock exposure fraction and sediment supply in channels with initial sediment cover.
 287 In a steeper slope channel ($S = 0.02$, Run 2-B), the bedrock is completely exposed when the
 288 sediment supply to transport capacity rate is less than 0.4. However, a linear relationship
 289 between the extent of sediment cover and sediment supply is exhibited when the sediment supply
 290 exceeds the threshold value ($q_s/q_c > 0.6$). This threshold sediment supply rate beyond which
 291 there is a linear relationship between sediment cover fraction and sediment supply ratio

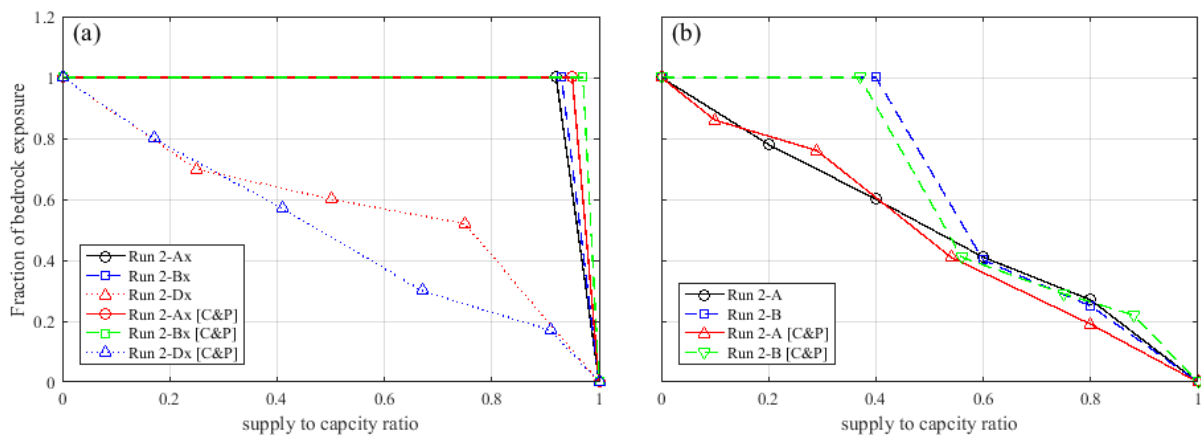


Figure 4. Results from the numerical simulations and flume experiments (Chatanantavet & Parker, 2008) of the fraction of bedrock exposure with varying sediment supply to transport capacity ratio for the simulations commenced from (a) bare bedrock channel and (b) alluvial channel.

292 decreases as the channel slope decreases (Run 2-A). In a channel slope of 0.0115, the linear
 293 relationship is observed throughout the entire range of q_s/q_c that the fraction of bedrock
 294 exposure increases gradually as the sediment supply to capacity ratio decreases.

295 3.3 Simulations with various initial sediment layer thickness

296 The simulations of Runs 2-B2 and 2-B2-a to 2-B2-c are conducted to explore the effect
 297 of antecedent sediment layer thickness on alluvial patterns. Figure 5 shows the time evolution of
 298 bedrock exposure and averaged alluvial thickness in the 2 % slope channel for both the
 299 simulations and Chatanantavet and Parker (2008) experiments. The initial sediment cover
 300 thickness was varied between 1 and 6 cm while the sediment flux of 66 g/s is constantly
 301 supplied. In the simulation starting with 1 cm sediment cover thickness, the sediment quickly
 302 erodes and washes out from the channel. The simulations with 2 cm or higher initial alluvial
 303 thickness present that the fraction of bedrock exposure increases gradually and converges
 304 approximately at 0.4. For those runs, the mean alluvial layer thickness over the sediment-covered
 305 area evolves toward 2 cm when the initial cover thickness equals or exceeds 2 cm.

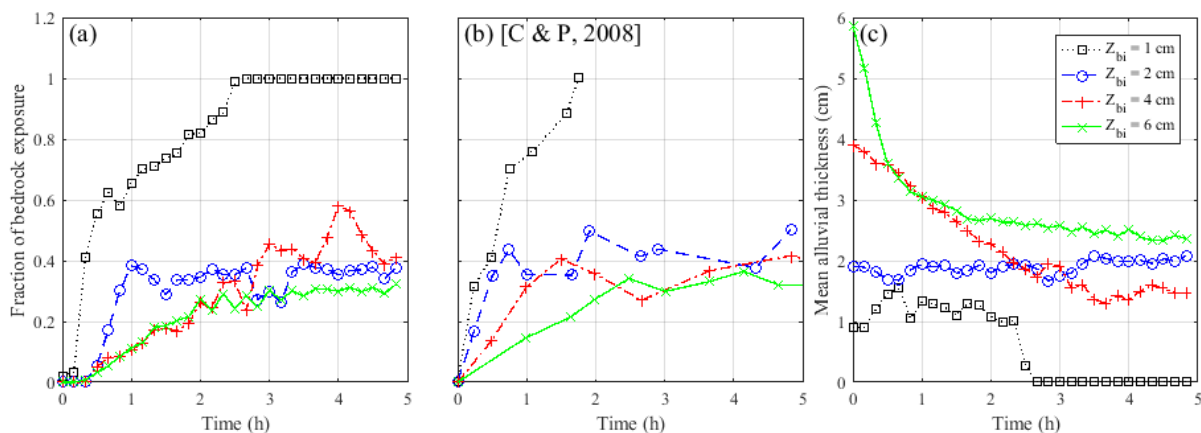


Figure 5. The time evolution of the (a) fraction of bedrock exposure from numerical simulations, (b) flume experiments (Chatanantavet & Parker, 2008), and (c) alluvial cover thickness averaged over the covered area only. The Runs of 2-B2-a, 2-B2, 2-B2-b, and 2-B2-c correspond to the initial cover thickness of 1, 2, 4, and 6 cm, respectively.

306 **4 Discussion**

307 Our results replicated several phenomena observed in the Chatanantavet & Parker (2008)
308 experiments: 1) runaway alluviation for high-slope channels with no initial sediment cover, and
309 gradual alluviation for low-slope channels with no initial sediment cover (Figure 4a), 2) a
310 threshold sediment supply for higher-slope channels with the initial cover below which sediment
311 washes out, but above which a linear relationship between sediment supply and fraction exposure
312 develops (Figure 4b), and 3) a threshold initial sediment cover thickness above which quasi-
313 steady sediment cover develops, but below which full bedrock exposure and sediment washout
314 occurs. The model's complete description of the hydrodynamic and sediment transport
315 conditions throughout the experiments help explain why these phenomena occurred.

316 4.1 Runaway alluviation vs. gradual alluviation

317 The gradual decrease in the fraction of bedrock exposed with increasing sediment supply
318 at the low-slope (2-Dx) condition, and the runaway alluviation at higher slopes where persistent
319 (total) sediment cover occurred only at sediment supply greater than the transport capacity, with
320 complete bedrock exposure at sediment supplies below that value, was observed in both our
321 numerical simulations and in the experiments of Chatanantavet and Parker (2008). Chatanantavet
322 and Parker (2008) suggested that this phenomenon may be in part due to sediment grain
323 interactions, such that at low slopes, frequent grain collisions lead to the development of alluvial
324 patches, which then increase local roughness and grow in size, whereas at higher slopes those
325 collisions may be less frequent and less likely to develop incipient patches. Hodge and Hoey's
326 (2012) cellular automata model runs with varying grain entrainment probability on bedrock and
327 alluvial surfaces suggest that the much higher grain entrainment probability on the bedrock
328 surface than the alluvial surface is a key factor of runaway alluviation.

329 Our model treats sediment transport as a continuum and is therefore not able to model
 330 grain interactions directly, but it still exhibited the same sort of slope-dependent relationship
 331 between gradual vs. runaway alluviation. Our model results suggest this is a result of the
 332 development of transcritical flows over bare low-slope beds, but not in higher-slope channels.

333 Figure 6 shows the Froude numbers calculated in the bare bedrock channel before
 334 feeding sediment at the inlet for the Runs 2-Ax, 2-Bx, and 2-Dx. The flow is supercritical in
 335 steep slope channels (2-Ax and 2-Bx), while locally subcritical flow is observed in lower slope
 336 channels (2-Dx). The flow field variables and shear stress result in a low sediment transport
 337 capacity where the flow is subcritical in the low-slope channel (Figure 7). These subcritical
 338 zones become areas of deposition, inducing a cascade of local changes in roughness, velocity,
 339 shear stress, and critical dimensionless shear stress which permit the growth of alluvial patches.
 340 However, in the steep slope channels, the large sediment transport capacity produced by high
 341 flow velocity and shear stress results in the particles passing through the channel reach without
 342 ever residing on the bed when the sediment supply is less than the transport capacity (Figure 4a).

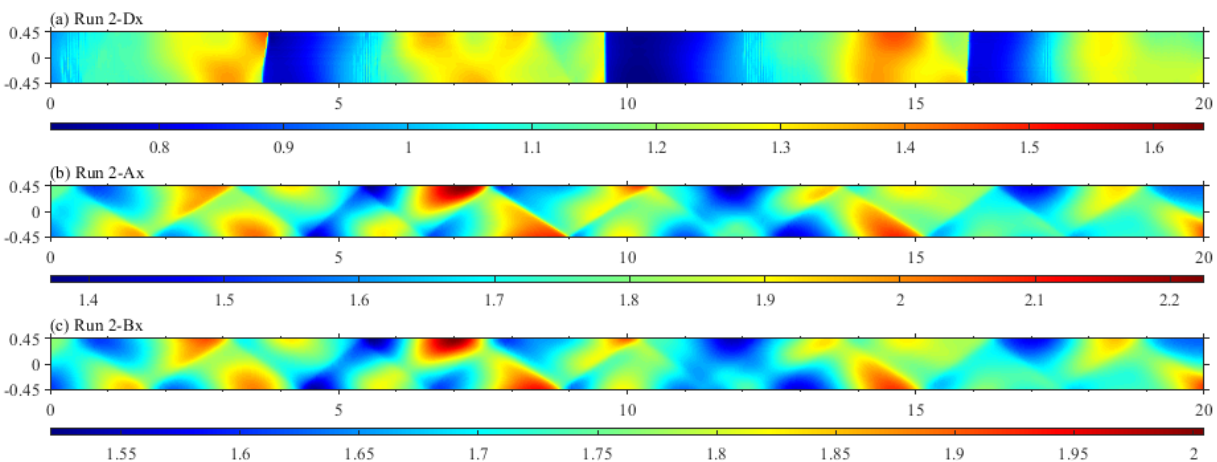


Figure 6. Initially calculated Froude number for Runs (a) 2-Dx, (b) 2-Ax, and (c) 2-Bx in bare bedrock channel. Colorbars indicate the scale of computed values, respectively.

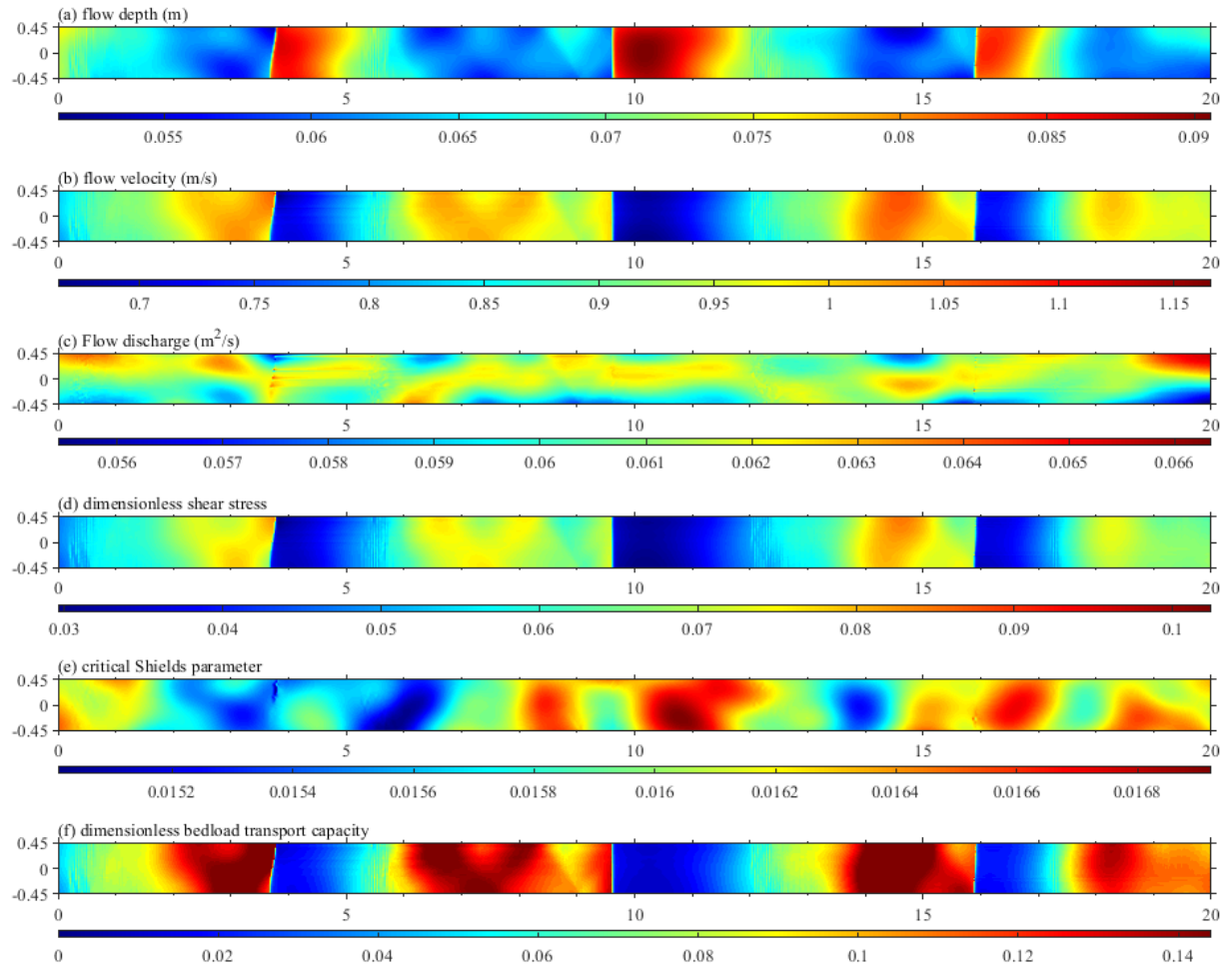


Figure 7. Initially calculated variables in bare bedrock channel for the Run 2-Dx: (a) flow depth, (b) flow velocity, (c) flow discharge, (d) dimensionless shear stress, (e) critical Shields parameter, and (f) dimensionless bedload transport capacity. Colorbars indicate the scale of computed values, respectively.

343 Thus, while grain interactions and roughness feedbacks may play a role in developing
 344 persistent alluvial sediment cover at below-capacity sediment supply in low-slope channels, the
 345 flow field – especially the presence of regions of transcritical flow – may be a necessary and
 346 important condition leading to this behavior.

347 4.2 Sediment supply threshold for persistent alluvial patches

348 The 2 % slope channel simulations with 2 cm initial cover thickness (Runs 2-B1, 2-B2, 2-
 349 B3, and 2-B4) show sediment washing out when the sediment supply rate is less than the

350 threshold capacity of about . The sediment forms alternate bars that produce additional
 351 resistance to the flow. The increased form drag roughness competes with decreased bed surface
 352 roughness due to exposed bedrock beds. The channel experiences complete bedrock exposure
 353 when the sediment supply does not meet the threshold amount to maintain the bedform. In other
 354 words, the sediment supplied to the system is redistributed to create bedforms which increase
 355 overall roughness and encourage sediment deposition and persistence of the alluvial cover; if the
 356 supply is insufficient to build the bedforms, the overall roughness decreases as bedrock becomes
 357 exposed and all of the sediment washes out (Figure 8).

358 Similar mechanisms explain the relationship between the initial thickness of sediment
 359 cover and the development of persistent alluvial cover as opposed to sediment washout at below-
 360 threshold initial thicknesses (Figure 5). The 1.15 % slope channel simulations with 1.5 cm initial
 361 cover thickness (Runs 2-A1 through 2-A5) show the linear relationship between the fraction
 362 cover and sediment supply to transport capacity. Transcritical flow is observed in this simulation
 363 (Figure 9). The flow is subcritical in the alluvial area and supercritical over the bedrock surface.
 364 The sediment forms a series of discrete sediment patches with a thin layer rather than a

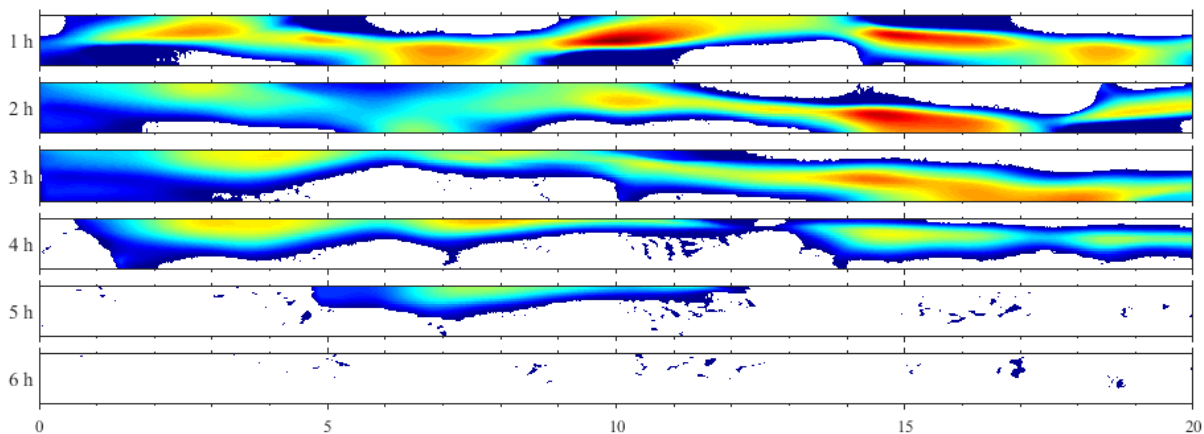


Figure 8. Simulated bed evolution of Run 2-B1 with $q_s/q_c = 0.4$. Colorbar shows the thickness of the sediment cover, and white areas correspond to the exposed bedrock surface.

365 continuous strip of sediment. The subcritical flow promotes the thin layer of alluvial patches to
 366 form even in low sediment supply channels.

367 Figure 10 shows how roughness changes from the initial value of grain and sediment
 368 transport roughness, form drag, and total hydraulic roughness through time. The non-bedform

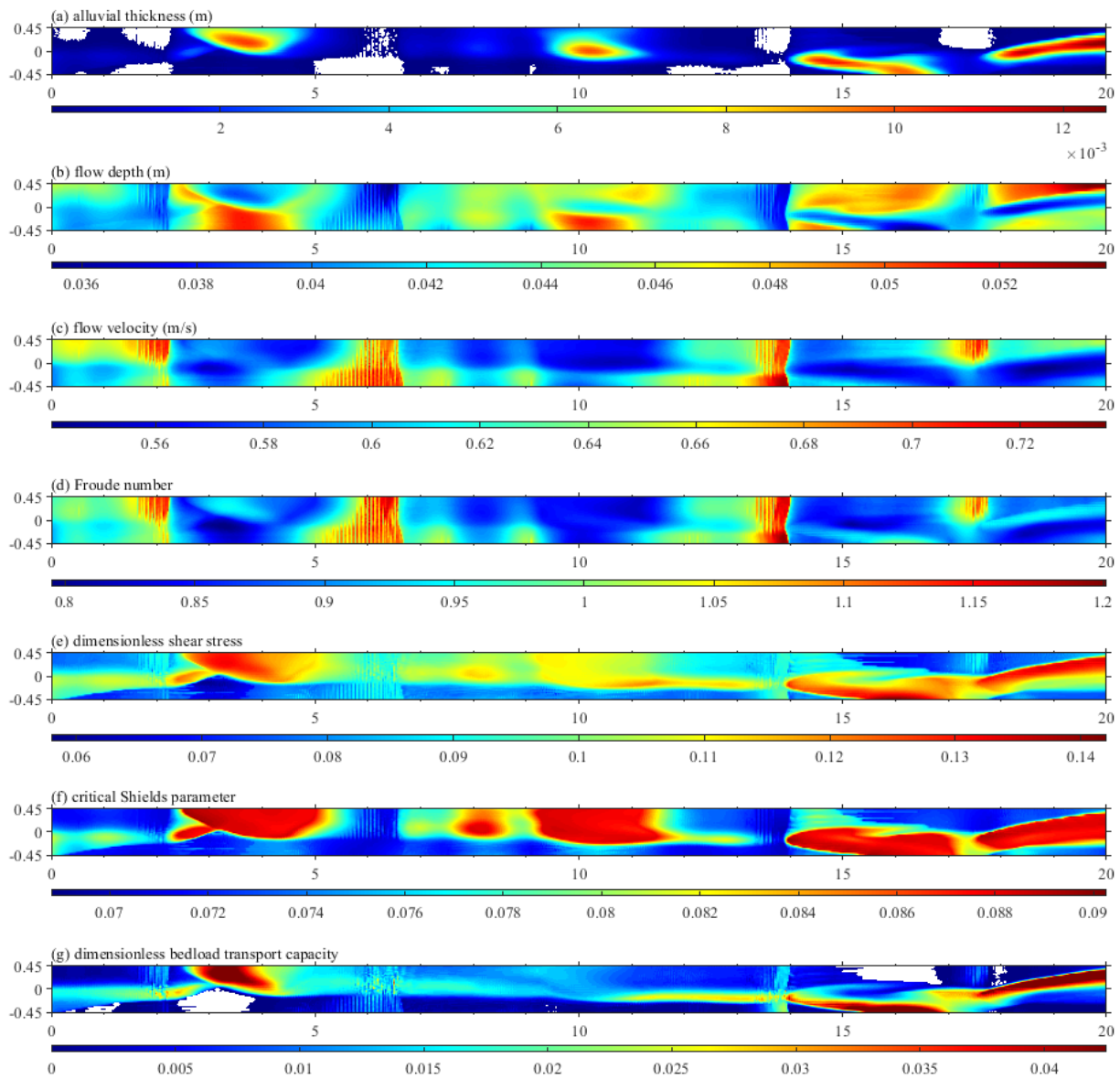


Figure 9. Simulation results commenced from alluvial channel for the Run 2-A2 at $t = 5$ h: (a) alluvial thickness, (b) flow depth, (c) flow velocity, (d) Froude number, (e) dimensionless shear stress, (f) critical Shields parameter, and (g) dimensionless bedload transport capacity. Colorbars indicate the scale of computed values, respectively. White areas correspond to (a) the exposed bedrock surface and (g) no bedload transport.

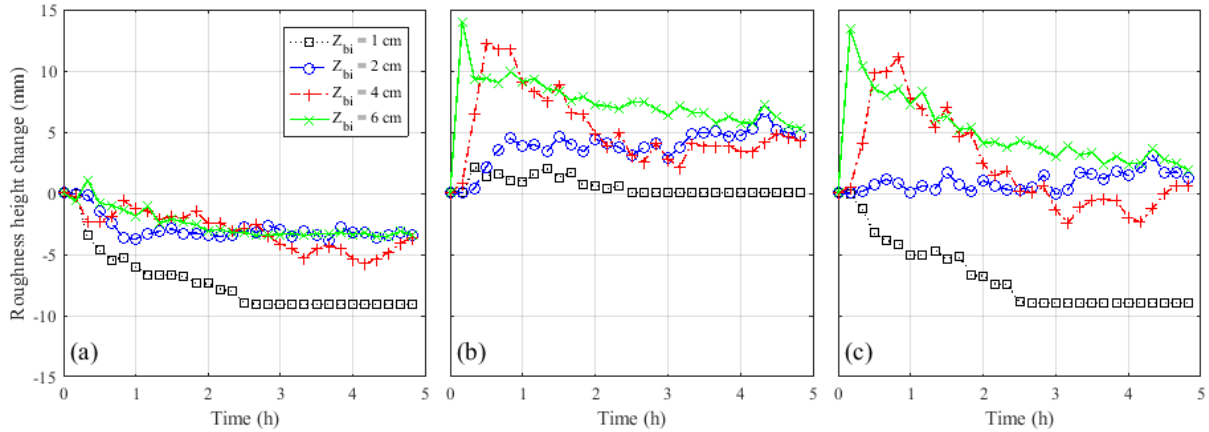


Figure 10. The time evolution of roughness difference from the initial roughness value: (a) bed surface roughness, (b) bedform roughness, and (c) total hydraulic roughness. The Runs of 2-B2-a, 2-B2, 2-B2-b, and 2-B2-c correspond to the initial cover thickness of 1, 2, 4, and 6 cm, respectively.

369 roughness gradually decreases as bedrock exposure increases for all Runs of 2-B2. However, the
 370 bedform roughness of Runs 2-B2, 2-B2-b, and 2-B2-c increases to 5 mm at the equilibrium state,
 371 whereas the bedform roughness of Run 2-B2-a increases at the early stage and decreases back to
 372 0. The changes in total roughness height indicate that the channel initially requires a thicker
 373 sediment cover layer than the threshold value to develop bars and maintain alluvial strips, or
 374 sediment washing out occurs.

375 5 Conclusions

376 We used a two-dimensional morphodynamic model to conduct a series of numerical
 377 experiments in the mixed bedrock-alluvial channel. This study explores the interaction between
 378 bedrock alluviation and morphological evolution. Simulations with varying sediment supply are
 379 conducted in different slope and antecedent channel conditions. The model replicated
 380 observations from a mixed bedrock-alluvial experiment (Chatanantavet & Parker, 2008),
 381 including a) the relationship between channel slope and gradual vs. runaway alluviation, b) the
 382 slope-dependent sediment supply threshold for development of persistent alluvial cover, c) the
 383 relationship between decreasing bedrock exposure and increasing sediment supply, and d) the

384 development of constant alluvial cover thickness regardless of initial sediment thickness,
385 provided the initial thickness exceeds a minimum value necessary to maintain bedform
386 dimensions.

387 The model results provide physical insight on the mechanisms responsible for these
388 phenomena. Transcritical flow plays an important role in initiating sediment deposition over
389 initially bare bedrock, and the development of transcritical zones in low-slope simulations but
390 not high-slope simulations may explain the apparent slope dependence of runaway alluviation.
391 Persistent sediment cover in high-slope channels is possible when rough alluvial surfaces balance
392 the extent of lower-roughness bedrock surfaces, and steeper channels require higher sediment
393 supply to exceed an apparent threshold where that balance can occur.

394 **Open Research**

395 The output data from numerical simulations used in this analysis can be found at
396 <https://github.com/rcemorpho/morph2d>.

397 **References**

398 Buffington, J. M., Montgomery, D. R., & Greenberg, H. M. (2004). Basin-scale availability of
399 salmonid spawning gravel as influenced by channel type and hydraulic roughness in
400 mountain catchments. *Canadian Journal of Fisheries and Aquatic Sciences*, *61*(11),
401 2085–2096. <https://doi.org/10.1139/f04-141>

402 Calantoni, J. (2002). Discrete particle model for bedload sediment transport in the surf zone. In
403 *ProQuest Dissertations and Theses*.
404 [https://search.proquest.com/docview/305510563?accountid=6180%0Ahttp://dw2zn6fm9](https://search.proquest.com/docview/305510563?accountid=6180%0Ahttp://dw2zn6fm9z.search.serialssolution.com?ctx_ver=Z39.88-2004&ctx_enc=info:ofi/enc:UTF-)
405 [z.search.serialssolution.com?ctx_ver=Z39.88-2004&ctx_enc=info:ofi/enc:UTF-](https://search.proquest.com/docview/305510563?accountid=6180%0Ahttp://dw2zn6fm9z.search.serialssolution.com?ctx_ver=Z39.88-2004&ctx_enc=info:ofi/enc:UTF-)

- 406 8&rft_id=info:sid/ProQuest+Dissertations+%26+Theses+Global&rft_val_fmt=info:ofi/f
407 mt:kev:mtx:dissertati
- 408 Chatanantavet, P., & Parker, G. (2008). Experimental study of bedrock channel alluviation under
409 varied sediment supply and hydraulic conditions. *Water Resources Research*, 44(12), 1–
410 19. <https://doi.org/10.1029/2007WR006581>
- 411 Demeter, G. I., Sklar, L. S., & Davis, J. R. (2005). The influence of variable sediment supply and
412 bed roughness on the spatial distribution of incision in a laboratory bedrock channel.
413 *2005 Fall Meeting of the AGU*, 2004.
- 414 Detert, M., & Parker, G. (2010). Estimation of the Washout Depth of Fine Sediments from a
415 Granular Bed. *Journal of Hydraulic Engineering*, 136(10), 790–793.
416 [https://doi.org/10.1061/\(ASCE\)HY.1943-7900.0000263](https://doi.org/10.1061/(ASCE)HY.1943-7900.0000263)
- 417 Duan, J. G., & Julien, P. Y. (2005). Numerical simulation of the inception of channel
418 meandering. *Earth Surface Processes and Landforms*, 30(9), 1093–1110.
419 <https://doi.org/10.1002/esp.1264>
- 420 Finnegan, N. J., Sklar, L. S., & Fuller, T. K. (2007). Interplay of sediment supply, river incision,
421 and channel morphology revealed by the transient evolution of an experimental bedrock
422 channel. *Journal of Geophysical Research: Earth Surface*, 112(3), 1–17.
423 <https://doi.org/10.1029/2006JF000569>
- 424 Hartshorn, K., Hovius, N., Dade, W. B., & Slingerland, R. L. (2002). Climate-driven bedrock
425 incision in an active mountain belt. *Science*, 297(5589), 2036–2038.
426 <https://doi.org/10.1126/science.1075078>

- 427 Hodge, R. A., & Hoey, T. B. (2012). Upscaling from grain-scale processes to alluviation in
428 bedrock channels using a cellular automaton model. *Journal of Geophysical Research:
429 Earth Surface*, 117(F1), n/a-n/a. <https://doi.org/10.1029/2011JF002145>
- 430 Hodge, R. A., & Hoey, T. B. (2016a). A Froude-scaled model of a bedrock-alluvial channel
431 reach: 1. Hydraulics. *Journal of Geophysical Research: Earth Surface*, 121(9), 1578–
432 1596. <https://doi.org/10.1002/2015JF003706>
- 433 Hodge, R. A., & Hoey, T. B. (2016b). A Froude-scaled model of a bedrock-alluvial channel
434 reach: 2. Sediment cover. *Journal of Geophysical Research: Earth Surface*, 121(9),
435 1597–1618. <https://doi.org/10.1002/2015JF003709>
- 436 Howard, A. D. (1980). Thresholds in river regimes. In *Thresholds in Geomorphology* (pp. 227–
437 258).
- 438 Howard, A. D., Dietrich, W. E., & Seidl, M. A. (1994). Modeling fluvial erosion on regional to
439 continental scales. *Journal of Geophysical Research: Solid Earth*, 99(B7), 13971–13986.
440 <https://doi.org/10.1029/94JB00744>
- 441 Howard, A. D., & Kerby, G. (1983). Channel changes in badlands. *Geological Society of
442 America Bulletin*, 94(6), 739. [https://doi.org/10.1130/0016-
443 7606\(1983\)94<739:CCIB>2.0.CO;2](https://doi.org/10.1130/0016-7606(1983)94<739:CCIB>2.0.CO;2)
- 444 Huston, D. L., & Fox, J. F. (2015). Clogging of Fine Sediment within Gravel Substrates:
445 Dimensional Analysis and Macroanalysis of Experiments in Hydraulic Flumes. *Journal
446 of Hydraulic Engineering*, 141(8), 1–14. [https://doi.org/10.1061/\(ASCE\)HY.1943-
447 7900.0001015](https://doi.org/10.1061/(ASCE)HY.1943-7900.0001015)

- 448 Huston, D. L., & Fox, J. F. (2016). Momentum-Impulse Model of Fine Sand Clogging Depth in
449 Gravel Streambeds for Turbulent Open-Channel Flow. *Journal of Hydraulic*
450 *Engineering*, 142(2). [https://doi.org/10.1061/\(ASCE\)HY.1943-7900.0001092](https://doi.org/10.1061/(ASCE)HY.1943-7900.0001092)
- 451 Inoue, T., Iwasaki, T., Parker, G., Shimizu, Y., Izumi, N., Stark, C. P., & Funaki, J. (2016).
452 Numerical Simulation of Effects of Sediment Supply on Bedrock Channel Morphology.
453 *Journal of Hydraulic Engineering*, 04016014. [https://doi.org/10.1061/\(ASCE\)HY.1943-](https://doi.org/10.1061/(ASCE)HY.1943-7900.0001124)
454 [7900.0001124](https://doi.org/10.1061/(ASCE)HY.1943-7900.0001124)
- 455 Inoue, T., Izumi, N., Shimizu, Y., & Parker, G. (2014). Interaction among alluvial cover, bed
456 roughness, and incision rate in purely bedrock and alluvial-bedrock channel. *Journal of*
457 *Geophysical Research: Earth Surface*, 119(10), 2123–2146.
458 <https://doi.org/10.1002/2014JF003133>
- 459 Johnson, J. P. L. (2014). A surface roughness model for predicting alluvial cover and bed load
460 transport rate in bedrock channels. *Journal of Geophysical Research: Earth Surface*,
461 *119Johnson*(10), 2147–2173. <https://doi.org/10.1002/2013JF003000>
- 462 Johnson, J. P. L., & Whipple, K. X. (2007). Feedbacks between erosion and sediment transport
463 in experimental bedrock channels. *Earth Surface Processes and Landforms*, 32(7), 1048–
464 1062. <https://doi.org/10.1002/esp.1471>
- 465 Johnson, J. P. L., & Whipple, K. X. (2010). Evaluating the controls of shear stress, sediment
466 supply, alluvial cover, and channel morphology on experimental bedrock incision rate. *J.*
467 *Geophys. Res.*, 115, F02018. <https://doi.org/10.1029/2009JF001335>
- 468 Kuhnle, R. A., Wren, D. G., Langendoen, E. J., & Rigby, J. R. (2013). Sand transport over an
469 immobile gravel substrate. *Journal of Hydraulic Engineering*, 139(2), 167–176.
470 [https://doi.org/10.1061/\(ASCE\)HY.1943-7900.0000615](https://doi.org/10.1061/(ASCE)HY.1943-7900.0000615)

- 471 Lamb, M. P., Dietrich, W. E., & Venditti, J. G. (2008). Is the critical shields stress for incipient
472 sediment motion dependent on channel-bed slope? *Journal of Geophysical Research:*
473 *Earth Surface*, 113(2), 1–20. <https://doi.org/10.1029/2007JF000831>
- 474 Lamb, M. P., Finnegan, N. J., Scheingross, J. S., & Sklar, L. S. (2015). New insights into the
475 mechanics of fluvial bedrock erosion through flume experiments and theory.
476 *Geomorphology*, 244, 33–55. <https://doi.org/10.1016/j.geomorph.2015.03.003>
- 477 Lisle, T. E., & Hilton, S. (1992). The Volume Of Fine Sediment In Pools: An Index Of Sediment
478 Supply In Gravel-Bed Streams. *Journal of the American Water Resources Association*,
479 28(2), 371–383. <https://doi.org/10.1111/j.1752-1688.1992.tb04003.x>
- 480 Lisle, T. E., & Lewis, J. (1992). Effects of Sediment Transport on Survival of Salmonid Embryos
481 in a Natural Stream: A Simulation Approach. *Canadian Journal of Fisheries and Aquatic*
482 *Sciences*, 49(11), 2337–2344. <https://doi.org/10.1139/f92-257>
- 483 Luu, L. X., Egashira, S., & Takebayashi, H. (2004). Investigation of Tan Chau Reach In Lower
484 Mekong Using Field Data And Numerical Simulation. *PROCEEDINGS OF*
485 *HYDRAULIC ENGINEERING*, 48(5), 1057–1062. <https://doi.org/10.2208/prohe.48.1057>
- 486 Madej, M. A. (2001). Development of channel organization and roughness following sediment
487 pulses in single-thread, gravel bed rivers. *Water Resources Research*, 37(8), 2259–2272.
488 <https://doi.org/10.1029/2001WR000229>
- 489 Massong, T. M., & Montgomery, D. R. (2000). Influence of sediment supply, lithology, and
490 wood debris on the distribution of bedrock and alluvial channels. *Geological Society of*
491 *America Bulletin*, 112(4), 591–599. [https://doi.org/10.1130/0016-](https://doi.org/10.1130/0016-7606(2000)112<591:IOSSLA>2.0.CO;2)
492 [7606\(2000\)112<591:IOSSLA>2.0.CO;2](https://doi.org/10.1130/0016-7606(2000)112<591:IOSSLA>2.0.CO;2)

- 493 McLean, S. R., Nelson, J. M., & Wolfe, S. R. (1994). Turbulence structure over two-dimensional
494 bed forms: Implications for sediment transport. *Journal of Geophysical Research*,
495 99(C6), 12729. <https://doi.org/10.1029/94JC00571>
- 496 Mishra, J., & Inoue, T. (2020). Alluvial cover on bedrock channels: applicability of existing
497 models. *Earth Surface Dynamics*, 8(3), 695–716. [https://doi.org/10.5194/esurf-8-695-](https://doi.org/10.5194/esurf-8-695-2020)
498 2020
- 499 Montgomery, D. R., Abbe, T. B., Buffington, J. M., Peterson, N. P., Schmidt, K. M., & Stock, J.
500 D. (1996). Distribution of bedrock and alluvial channels in forested mountain drainage
501 basins. In *Nature* (Vol. 381, Issue 6583, pp. 587–589). <https://doi.org/10.1038/381587a0>
- 502 Montgomery, D. R., & Buffington, J. M. (1997). Channel-reach morphology in mountain
503 drainage basins. *Bulletin of the Geological Society of America*, 109(5), 596–611.
504 [https://doi.org/10.1130/0016-7606\(1997\)109<0596:CRMIMD>2.3.CO](https://doi.org/10.1130/0016-7606(1997)109<0596:CRMIMD>2.3.CO)
- 505 Nelson, J. M., Bennett, J. P., & Wiele, S. M. (2003). Flow and sediment-transport modeling.
506 *Tools in Fluvial Geomorphology*. <https://doi.org/10.1002/0470868333.ch18>
- 507 Ribberink, J. S. (1987). Mathematical modelling of one-dimensional morphological changes in
508 rivers with non-uniform sediment. *Communications on Hydraulic & Geotechnical*
509 *Engineering - Delft University of Technology*, 87–2.
- 510 Sklar, L., & Dietrich, W. (1998). River longitudinal profiles and bedrock incision models:
511 Stream power and the influence of sediment supply. In K. J. Tinkler & E. E. Wohl (Eds.),
512 *Rivers Over Rock: Fluvial Processes in Bedrock Channels* (Volume 107, pp. 237–260).
513 <https://doi.org/10.1029/GM107p0237>

- 514 Sklar, L., & Dietrich, W. (2001). Sediment and rock strength controls on river incision into
515 bedrock. *Geology*, 29(12), 1087. [https://doi.org/10.1130/0091-](https://doi.org/10.1130/0091-7613(2001)029<1087:SARSCO>2.0.CO;2)
516 [7613\(2001\)029<1087:SARSCO>2.0.CO;2](https://doi.org/10.1130/0091-7613(2001)029<1087:SARSCO>2.0.CO;2)
- 517 Sklar, L., & Dietrich, W. (2004). A mechanistic model for river incision into bedrock by
518 saltating bed load. *Water Resources Research*, 40(6), 1–21.
519 <https://doi.org/10.1029/2003WR002496>
- 520 Soulsby, R. (1997). Dynamics of Marine Sands. In *Dynamics of Marine Sands*. Thomas Telford
521 Ltd. <https://doi.org/10.1680/DOMS.25844>
- 522 Struiksma, N. (1985). Prediction of 2-D bed topography in rivers. *Journal of Hydraulic*
523 *Engineering*, 111(8), 1169–1182. [https://doi.org/10.1061/\(ASCE\)0733-](https://doi.org/10.1061/(ASCE)0733-9429(1985)111:8(1169))
524 [9429\(1985\)111:8\(1169\)](https://doi.org/10.1061/(ASCE)0733-9429(1985)111:8(1169))
- 525 Talmon, A. M., Struiksma, N., & Van Mierlo, M. C. L. M. (1995). Laboratory measurements of
526 the direction of sediment transport on transverse alluvial-bed slopes. *Journal of*
527 *Hydraulic Research*, 33(4), 495–517. <https://doi.org/10.1080/00221689509498657>
- 528 Toro, E. F. (1992a). The weighted average flux method applied to the Euler equations.
529 *Philosophical Transactions of the Royal Society of London. Series A: Physical and*
530 *Engineering Sciences*, 341(1662), 499–530. <https://doi.org/10.1098/rsta.1992.0113>
- 531 Toro, E. F. (1992b). Riemann Problems and the WAF Method for Solving the Two-Dimensional
532 Shallow Water Equations. *Philosophical Transactions of the Royal Society A:*
533 *Mathematical, Physical and Engineering Sciences*, 338(1649), 43–68.
534 <https://doi.org/10.1098/rsta.1992.0002>
- 535 Tubino, M., Repetto, R., & Zolezzi, G. (1999). Free bars in rivers. *Journal of Hydraulic*
536 *Research*, 37(6), 759–775. <https://doi.org/10.1080/00221689909498510>

- 537 Turowski, J. M., Hovius, N., Meng-Long, H., Lague, D., & Men-Chiang, C. (2008). Distribution
538 of erosion across bedrock channels. *Earth Surface Processes and Landforms*, 33(3), 353–
539 363. <https://doi.org/10.1002/esp.1559>
- 540 Turowski, J. M., Hovius, N., Wilson, A., & Horng, M. J. (2008). Hydraulic geometry, river
541 sediment and the definition of bedrock channels. *Geomorphology*, 99(1–4), 26–38.
542 <https://doi.org/10.1016/j.geomorph.2007.10.001>
- 543 Turowski, J. M., Lague, D., & Hovius, N. (2007). Cover effect in bedrock abrasion: A new
544 derivation and its implications for the modeling of bedrock channel morphology. *Journal*
545 *of Geophysical Research: Earth Surface*, 112(4), 1–16.
546 <https://doi.org/10.1029/2006JF000697>
- 547 Vermeer, K. (1986). The ripple factor in sediment transport equations. *Rep. R657/M1314-V*.
- 548 Wong, M., Parker, G., DeVries, P., Brown, T. M., & Burges, S. J. (2007). Experiments on
549 dispersion of tracer stones under lower-regime plane-bed equilibrium bed load transport.
550 *Water Resources Research*, 43(3), n/a-n/a. <https://doi.org/10.1029/2006WR005172>
- 551 Zhang, L., Parker, G., Stark, C., Inoue, T., Viparelli, E., Fu, X., & Izumi, N. (2015). Macro-
552 roughness model of bedrock-alluvial river morphodynamics. *Earth Surface Dynamics*,
553 3(1), 113–138. <https://doi.org/10.5194/esurf-3-113-2015>

15 **Abstract**

16 Understanding the development and spatial distribution of alluvial patches in mixed bedrock-
17 alluvial rivers is necessary to predict the mechanisms of the interactions between sediment
18 transport, alluvial cover, and bedrock erosion. This study aims to analyze patterns of bedrock
19 alluviation using a 2D morphodynamic model, and to use the model results to better understand
20 the mechanisms responsible for alluvial patterns observed experimentally. A series of
21 simulations are conducted to explore how alluvial patterns in mixed bedrock-alluvial channels
22 form and evolve for different channel slopes and antecedent sediment layer thicknesses. In
23 initially bare bedrock low-slope channels, the model predicts a linear relationship between
24 sediment cover and sediment supply because areas of subcritical flow enable sediment
25 deposition, while in steep-slope channels the flow remains fully supercritical and the model
26 predicts so-called runaway alluviation. For channels initially covered with sediment, the model
27 predicts a slope-dependent sediment supply threshold above which a linear relationship between
28 bedrock exposure and sediment supply develops, and below which the bedrock becomes fully
29 exposed. For a given sediment supply, the fraction of bedrock exposure and average alluvial
30 thickness converge toward the equilibrium value regardless of the initial cover thickness so long
31 as it exceeds a minimum threshold. Steep channels are able to maintain a continuous strip of
32 sediment under sub-capacity sediment supply conditions by achieving a balance between
33 increased form drag as bedforms develop and reduced surface roughness as the portion of
34 alluvial cover decreases. In lower-slope channels, alluvial patches are distributed sporadically in
35 regions of the subcritical flow.

36 **Plain Language Summary**

37 Bedrock rivers may have patches of alluvial sediment that covers some or all of the underlying
38 bedrock. The amount of this sediment cover can change dynamically over time depending on the
39 flow, upstream sediment supply, channel morphology, and antecedent sediment conditions. Here,
40 we use a numerical model to simulate flow and sediment transport so that we may better
41 understand what controls sediment cover in mixed bedrock-alluvial rivers. We use the model to
42 simulate channels of varying slopes, sediment supplies, and initial sediment cover, and we
43 analyze the model's output to gain insight on how alluvial patches form and what controls their
44 extent and dynamics. Our numerical model results produce phenomena that have been observed
45 in physical experiments, and they show that the channel slope and initial sediment thickness
46 plays an important role in determining whether and how much sediment can be deposited. Our
47 results also show that flow transitions provide critical locations where sediment deposits can start
48 to form. Persistent sediment cover in bedrock channels can develop when a delicate equilibrium
49 is reached between sediment roughness and the flow field.

50 **1 Introduction**

51 Bedrock channels are characterized by occasional or continuous exposures of
52 nonalluviated bedrock, which is a consequence of these channels receiving a sediment supply
53 that is less than their transport capacity. A wide variety of models for drainage network evolution
54 distinguish between bedrock and alluvial reaches (Howard, 1980; Howard et al., 1994; Howard
55 & Kerby, 1983; Montgomery et al., 1996) by using channel slope and discharge to express
56 channel transport capacity. Field investigations (Lamb et al., 2008; Massong & Montgomery,
57 2000; Montgomery et al., 1996; Montgomery & Buffington, 1997) demonstrate that bedrock
58 channels occur at slopes greater than a critical value ($S > S_c$), and alluvial channels form at a
59 slope less than the critical value ($S \leq S_c$).

60 The spatial distribution of alluvial cover in mixed bedrock-alluvial channels has
61 importance for determining rates and patterns of bedrock erosion, hydrodynamics, and aquatic
62 habitat. Mechanistic models of bedrock erosion incorporate the erosional mechanism of saltating
63 bedload particles impacting and eroding bedrock (e.g., Demeter et al., 2005; Hartshorn et al.,
64 2002; Sklar & Dietrich, 1998, 2001, 2004; Zhang et al., 2015), implicitly introducing
65 dependence on sediment supply and bedrock exposure into the calculation of erosion rates.
66 Competition between the tools and cover effects controls the spatial distribution of the bedrock
67 channel erosion, resulting in lateral and vertical channel erosion and meandering (Finnegan et al.,
68 2007; Lamb et al., 2015; Turowski et al., 2007; Turowski, Hovius, Meng-Long, et al., 2008;
69 Turowski, Hovius, Wilson, et al., 2008). The cover effect is typically demonstrated by linear or
70 exponential relations of fractional bedrock exposure as a function of sediment supply to transport
71 capacity ratio (Sklar & Dietrich, 1998, 2004; Turowski et al., 2007). Additionally, sediment
72 supply and alluvial cover impact the maintenance and distribution of aquatic habitat and attached
73 micro-organisms (Buffington et al., 2004; Detert & Parker, 2010; Huston & Fox, 2015, 2016;
74 Kuhnle et al., 2013; Lisle & Hilton, 1992; Lisle & Lewis, 1992; Madej, 2001).

75 Alluvial patterns in bedrock channels are controlled by spatial and temporal variations in
76 sediment flux, transport capacity, and bed topography. These channels can exhibit alluvial
77 patterns ranging from continuous and concentrated longitudinal strips of sediment to spatially
78 discontinuous patches of sediment. Experiments in mixed bedrock-alluvial channels have
79 observed spatially concentrated sediment cover and storage in low parts of the underlying
80 bedrock topography (Finnegan et al., 2007; Johnson & Whipple, 2007), indicating that
81 topographic roughness induces changes in local flow properties and threshold of sediment
82 motion. Inoue et al. (2014) observed inconsistent development of alluvial cover in the inner

83 channel through their field experiments. Hodge and Hoey's (2016a, 2016b) experiments show
84 that velocity is an important control on sediment deposition, as they did not observe sediment
85 cover at low areas of the bed where the flow velocity remained high. The results from several
86 experimental studies (Chatanantavet & Parker, 2008; Johnson & Whipple, 2010; Sklar &
87 Dietrich, 2004; Turowski et al., 2007) suggest a few major factors control grain entrainment and
88 bedrock exposure, such as sediment supply rate, channel slope, material size, and bed roughness.

89 A set of flume experiments (Chatanantavet & Parker, 2008) using different channel bed
90 slopes has shown that for lower slopes ($S < 0.0115$) bedrock exposure decreased more or less
91 linearly with increasing the ratio of sediment supply rate to capacity transport rate. However, for
92 sufficiently higher slopes ($S \geq 0.0115$), the bedrock remained fully exposed when the ratio of
93 sediment supply to transport capacity is less than a critical value, while a linear relationship
94 between the degree of bedrock exposure and sediment supply rate to transport capacity ratio
95 prevailed when the sediment supply exceeds transport capacity. These experiments also
96 documented a slope-dependent “runaway alluviation,” where for initially bare-bedrock
97 conditions, low-slope channels develop linearly increasing sediment cover with increasing
98 sediment supply, while high-slope channels remain completely exposed until sediment supply
99 exceeds the transport capacity, beyond which the channel becomes fully alluviated.

100 Chatanantavet and Parker (2008) suggested this may be a result of slope-dependent grain
101 interactions; later experiments by Mishra and Inoue (2020) indicated that runaway alluviation
102 occurred when the bedrock roughness was lower than the sediment roughness, but the gradual
103 alluvial cover could develop when the bedrock roughness was higher than that of the sediment. A
104 full explanation of the slope-dependent behavior of sediment dynamics in mixed bedrock-
105 alluvial channels is still needed.

106 Morphodynamic models have struggled to replicate the types of observations made in
107 mixed bedrock-alluvial experiments. Promising results have been presented by Hodge and Hoey
108 (2012), who developed a cellular automaton (CA) model where the probability of entrainment of
109 individual grains was specified for bedrock or alluvial areas. Their model found relationships
110 between bedrock exposure and the ratio of sediment supply to transport capacity (q_s/q_c) similar to
111 those observed by Chatanantavet and Parker (2008), but in contrast to the experimental
112 observations, the majority of their CA model runs predicted that the presence or absence of
113 sediment cover on the bed at the beginning of the run did not affect the steady state sediment
114 cover. Additionally, the entrainment probabilities needed to change from run to run for their
115 results to achieve the diversity of findings Chatanantavet and Parker (2008) reported. While CA
116 models like this provide interesting insight on the potential importance of grain dynamics for
117 alluvial patterns in bedrock-alluvial channels, the absence of a flow model makes connecting
118 probabilities of sediment entrainment and deposition to physical mechanisms of sediment
119 transport and alluviation challenging.

120 Because of the complexity inherent in the roughness relationship incorporated to the flow
121 resistance and sediment transport, evaluating the relative influence of different roughness
122 mechanisms for channel evolution is currently a challenging problem. The patterns of sediment
123 cover over the bedrock bed affect the spatial distribution of local roughness, flow rate, and
124 sediment transport. Here we use a new morphodynamic model to reproduce many of the
125 phenomena that have been observed in mixed bedrock-alluvial channels, and we use the model
126 predictions to untangle the mechanisms responsible for the range of dynamic sediment behavior
127 in these environments. In particular, we use the model to investigate the following questions: 1)
128 what explains the apparent slope dependence for runaway alluviation? 2) How can mixed

129 bedrock-alluvial channels maintain alluvial cover when the sediment supply is less than the
130 transport capacity? 3) How do initial conditions of sediment cover affect the temporal
131 development of alluvial cover, and the overall relationship between bedrock exposure and
132 sediment supply? Our results reveal the important interactions between dynamic channel
133 roughness, flow patterns, sediment transport rates, bedform development, and alluvial cover.

134 **2 Methods**

135 2.1 Morphodynamic model

136 We have developed a two-dimensional numerical morphodynamic model for mixed
137 bedrock-alluvial channels. The model is fully described in Cho and Nelson (submitted), and we
138 summarize the key aspects of the model here. The model consists of three major components: (1)
139 the 2D shallow water equations (SWE) in the depth-averaged form are applied to solve the
140 hydrodynamical component, (2) a sediment transport model calculates bedload transport rates
141 associated with the hydrodynamic variables and topographic variation, and (3) the modified
142 Exner equation, which computes changes in alluvial concentration or thickness due to sediment
143 transport divergence. The novel aspects of this model, compared to previous models applied to
144 mixed bedrock-alluvial morphodynamics, are 1) the Exner equation of sediment continuity
145 accounts for the volume of bedload in transport and the fraction of bed covered in sediment, 2) a
146 composite alluvial and bedrock roughness is used in the flow calculation, 3) the friction for
147 sediment transport is modified to account for the effects of bedforms, and 4) the numerical
148 scheme is robust and capable of handling Froude transitions and capturing shocks. We
149 summarize the key components of the model below.

150 A key assumption in most numerical models combining water flow, sediment transport,
151 and morphological evolution is that the response time of bed evolution is relatively long
152 compared to the timescales of relevance to the flow of water (McLean et al., 1994; Nelson et al.,
153 2003; Tubino et al., 1999). This allows a decoupling between the water flow computation and the
154 sediment equation by assuming a quasi-steady approximation of morphodynamic process that the
155 bed level does not change rapidly during an infinitesimal time interval while the flow field
156 adapts instantaneously. Thus, the decoupled model practically solves for the flow field and
157 topographic evolution using an iterative procedure.

158 Mixed bedrock-alluvial channels exhibit complex roughness feedbacks due to differential
159 roughness of alluvium and bedrock surfaces, the development of bedforms and associated form
160 drag, as well as bed shear stress taken up by sediment transport itself. To account for this, our
161 model uses a composite roughness partitioned into surface roughness of alluvial and bedrock
162 bed, sediment transport roughness, and form drag. The ripple factor is applied to the shear stress
163 to remove the form drag of the bedforms assuming the remaining part is responsible for sediment
164 transport.

165 Water depth and flux are calculated using the Harten-Lax-van Leer-Contract (HLLC)
166 scheme with the weighted average flux (WAF) method (Toro, 1992a, 1992b) and an explicit
167 application of the central difference of the viscous and friction terms at each computational cell
168 center in a 2D domain. Because of the local and global change in flow resistance associated with
169 different substrate roughness between the bedrock and bed material and bedform evolution, a
170 treatment of transcritical flow is necessary. The flow resistance consists of skin friction, form
171 drag, and bedload transport roughness. A linear fractional cover model representing the relation
172 between the alluvial bed and bare bedrock bed, the volume of local bed material per volume of a

173 monolayer of sediment grains, is used to calculate local skin friction. The form drag effect is
 174 determined using the local bed slope and topographic variation averaged over the area of interest.
 175 Additionally, the bedload layer thickness is added to the total roughness where the sediment
 176 transport occurs. The explicit calculation of each of these components of roughness is critical to
 177 be able to replicate observations of persistent sediment cover in mixed bedrock-alluvial channels
 178 (Cho and Nelson, submitted).

179 The bed morphology is updated using the modified Exner equation for sediment
 180 continuity (Inoue et al., 2014, 2016; Luu et al., 2004). The sediment transport capacity on the
 181 alluvial bed is estimated from Wong et al. (2007). A correction of the bedload transport rate on
 182 the pure bedrock bed is necessary considering a relatively small volume of bedload transport:

$$183 \quad q_b = \begin{cases} \frac{V_b}{V_{bc}} q_{bc} & \text{for } 0 \leq V_b < V_{bc} \\ q_{bc} & \text{for } V_{bc} \leq V_b \end{cases} \quad (1)$$

184 where q_b is the bedload transport rate per unit width, q_{bc} is the bedload transport capacity per
 185 unit width, V_b is the volume of sediment per unit area in the bedload layer, and V_{bc} is the
 186 saturation volume per unit area in the bedload layer. When the bed is completely bare, only the
 187 volume of sediment in the bedload layer is brought into bedload transport without resting on the
 188 bed, referred to as the throughput bedload. When the volume of the bedload layer exceeds the
 189 saturation value, sediment starts to deposit on the bed and the linear cover fraction model is
 190 utilized to determine whether the bed is in the state of partial or complete cover:

$$191 \quad \eta_a = \begin{cases} \frac{V_{ba} - V_{bc}}{1 - \lambda} & \text{for } V_{bc} \leq V_{ba} \\ 0 & \text{for } 0 \leq V_{ba} < V_{bc} \end{cases} \quad (2)$$

192 where η_a is the alluvial layer thickness, V_{ba} is the total volume of sediment per unit area in
 193 alluvial bedload layers, λ is the porosity, and

$$194 \quad V_b = \begin{cases} V_{bc} & \text{for } V_{bc} \leq V_{ba} \\ V_{ba} & \text{for } 0 \leq V_{ba} < V_{bc} \end{cases} \quad (3)$$

195 where $V_{bc} = q_{bc}/u_s$ and u_s is the saltation velocity.

196 The skin friction is used for the calculation of dimensionless shear stress to account for
 197 the fact that only the near-bed grain roughness is responsible for the sediment transport, using a
 198 correction referred as to the ripple factor (Ribberink, 1987; Vermeer, 1986). The dimensionless
 199 shear stress (Struiksma, 1985; Talmon et al., 1995) and critical Shields number (Calantoni, 2002;
 200 Duan & Julien, 2005; Soulsby, 1997) are corrected for spatially varying bed topography in the
 201 direction of flow.

202 The critical Shields parameter calculated as a function of the ratio of the bedrock
 203 hydraulic roughness to the grain size (Inoue et al., 2014; Johnson, 2014; Mishra & Inoue, 2020)
 204 is adopted instead of constant value for bedrock and alluvial surfaces. We use a modified
 205 dimensionless critical shear stress model to simulate bed evolution in different channel slopes:

$$206 \quad \tau_c^* = \alpha_c (k_0/d)^{0.6} \quad (4)$$

207 where α_c is the correction factor for different channel slopes, k_0 is the hydraulic roughness
 208 height, and d is the grain size.

209 2.2 Simulation conditions

210 We conducted a set of numerical experiments to explore how channel slope, initial
 211 sediment cover thickness, and sediment supply impact the evolution of patterns of alluvial cover

212 in mixed bedrock-alluvial channels. The simulations were designed to complement the
213 experiments of Chatanantavet and Parker (2008) and provide mechanistic insight into controls on
214 alluvial patterns in bedrock channels. Table 1 summarizes the initial flow and sediment condition
215 used in each experiment based on the flume experiments conducted by Chatanantavet and Parker
216 (2008). The computational channel is straight and longer than the experimental channel to avoid
217 possible problems regarding bedform development sensitive to boundary disturbances. All
218 simulations impose constant water and sediment supply, uniform sediment size, and non-erodible
219 bedrock to exclude potential disturbances to bed topography created by unsteady conditions. The
220 computations are stopped when near equilibrium conditions of bed topography are achieved, in
221 which the average sediment cover thickness and the fraction of bedrock cover vary around stable
222 values.

223 All simulations are performed in a rectangular bedrock channel having a length of 20 m
224 and a width of 0.9 m. Small topographic variations with a standard deviation of 2.2 mm and
225 peak-to-peak bed elevation of 9 mm are applied to the bedrock bed. First, two sets of simulations
226 are performed: (1) with some initial cover thickness with different channel slopes (Runs 2-A5
227 and 2-B5) and (2) without antecedent sediment cover (Runs 2-Ax, 2-Bx, and 2-Dx) to explore
228 the effect of channel slopes. Second, a set of Run 2-B is conducted with the $q_s/q_c = 0.6$ and
229 various initial sediment cover thicknesses of 1, 4, and 6 cm. Two types of uniform grains, fine 2
230 mm and coarse 7 mm gravels, are employed in the experiments with a mild slope channel (
231 $S \leq 0.0115$) and with a steep slope channel ($S = 0.02$), respectively.

Table 1. Summary of Flow, Sediment Transport, and Topographic Conditions^a

	mm		%	cm	l/s	g/s	g/s		mm	cm	cm/s	
RUN	k_b	α_c	S	Z_{bi}	Q_w	Q_c	Q_s	Q_s/Q_c	d	H	U	F_e
2-A1	0.4	0.03	1.15	1.5	24	25	5	0.2	2	4.3	62	0.78
2-A2	0.4	0.03	1.15	1.5	24	25	10	0.4	2	4.3	62	0.6
2-A3	0.4	0.03	1.15	1.5	24	25	15	0.6	2	4.3	62	0.41
2-A4	0.4	0.03	1.15	1.5	24	25	20	0.8	2	4.3	62	0.27
2-A5	0.4	0.03	1.15	1.5	24	25	25	1.0	2	4.5	59	0
2-B1	4	0.05	2	2	55	110	44	0.4	7	5	122	1
2-B2	4	0.05	2	2	55	110	66	0.6	7	5.5	111	0.4
2-B3	4	0.05	2	2	55	110	88	0.8	7	5.5	111	0.25
2-B4	4	0.05	2	2	55	110	110	1.0	7	6	102	0
2-B2-a	4	0.05	2	1	55	110	66	0.6	7	5	122	1
2-B2-b	4	0.05	2	4	55	110	66	0.6	7	6	102	0.4
2-B2-c	4	0.05	2	6	55	110	66	0.6	7	6	102	0.4
2-Ax	0.4	0.03	1.15	0	24	150	150	1.0	2	2.9	92	0
2-Bx	4	0.05	2	0	55	350	350	1.0	7	5	122	0
2-Dx-a	0.2	0.08	0.3	0	55	8	2	0.25	2	7.5	81	0.7
2-Dx-b	0.2	0.08	0.3	0	55	8	4	0.5	2	7.5	81	0.6
2-Dx-c	0.2	0.08	0.3	0	55	8	6	0.75	2	7.5	81	0.52
2-Dx-d	0.2	0.08	0.3	0	55	8	8	1.0	2	7.5	81	0

^aThe run names correspond to Chatanantavet and Parker's (2008) experimental conditions. k_b denotes bedrock roughness height, α_c denotes Shields number correction coefficient, S denotes channel slope, Z_{bi} denotes initial sediment cover thickness, Q_w denotes water discharge, Q_c denotes sediment transport capacity, Q_s denotes sediment supply rate, q_s/q_c denotes the ratio of sediment supply to transport capacity, d denotes grain size, H denotes flow depth, U denotes flow velocity, and F_e denotes the fraction of bedrock exposure, respectively.

232 The bedrock and grain roughness heights are back-calculated from the logarithmic law
233 depending on the channel slope and corresponding hydraulic conditions. The spatially varying
234 friction coefficient is then calculated as a function of the flow depth and composite roughness,
235 which depends upon the local status of fraction cover, bedform dimension, and bedload transport

236 rate. The critical Shields parameters for each channel slope are back-calculated by equating the
237 sediment transport capacity from our numerical simulations and experimental runs of
238 Chatanantavet and Parker (2008) conducted in bedrock channels, and adjustment to the
239 correction coefficient α_c is employed.

240 In each simulation, the sediment supply q_s was specified as a target fraction of the
241 transport capacity q_c . To determine q_c , we conducted simulations for each run, assuming that
242 the initial bed is nearly flat for either with initial sediment cover (Runs 2-A and 2-B) or bare
243 bedrock surface (Runs 2-Ax, 2-Bx, and 2-Dx) without the presence of bedforms. The bedrock
244 transport capacity is the lowest rate of sediment input per unit width fed into the initially bare
245 bedrock bed that results in equilibrium conditions where the bed is completely covered ($F_e = 0$).
246 The alluvial transport capacity is the channel averaged sediment transport rate in the alluvial
247 channel.

248 **3 Results**

249 **3.1 Simulations with no initial alluvial cover**

250 Runs 2-Ax, 2-Bx, and 2-Dx all commenced with a bare bedrock bed, and are used to
251 investigate how channel slope affects sudden vs. gradual alluviation as sediment supply
252 increases. The lowest-slope simulations ($S = 0.003$) of Run 2-Dx exhibited a gradual decrease in
253 bedrock exposure at increasing sediment supplies. An example of bed evolution for these runs is
254 shown in Figure 1 for Run 2-Dx-a, for which bedrock surface roughness was 0.2 mm and the
255 ratio of sediment supply to transport capacity was $q_s/q_c = 0.25$. The time evolution of alluvial
256 cover illustrates that the sediment grains initially deposit in the lower topography areas, and
257 sediment patches gradually grow thicker and expand in the upstream direction.

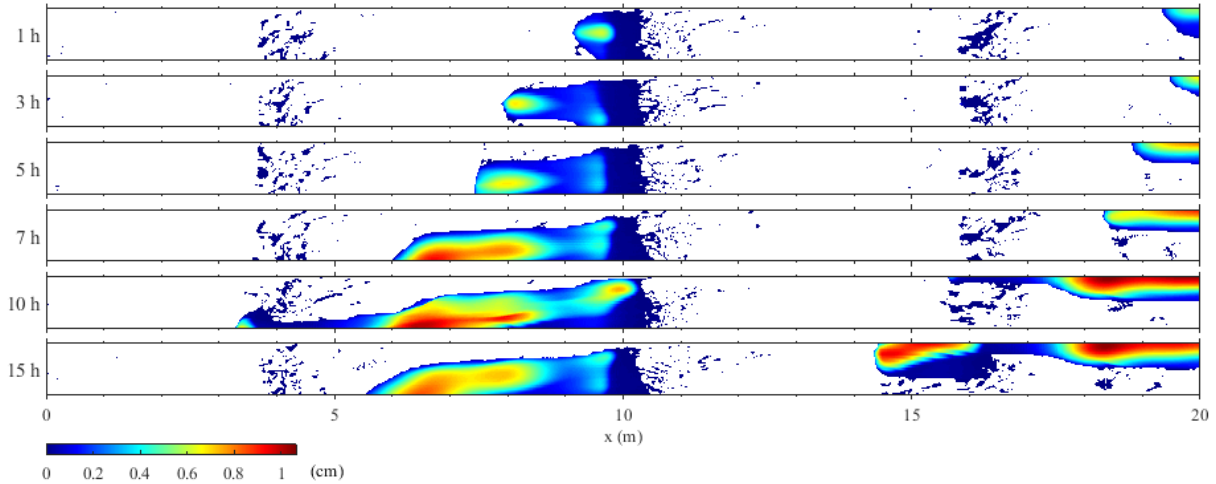


Figure 2. Simulated bed evolution of Run 2-Dx-a, which began with a bare bedrock bed and sediment supplied at $q_s/q_c = 0.25$. Colorbar shows the thickness of the sediment cover, and white areas correspond to the exposed bedrock surface.

258 Figure 2 shows the final state of alluviation for all of the low-slope 2-Dx runs. As

259 sediment supply (i.e., q_s/q_c) increases, the alluviated patches grow in size and the overall

260 fraction of exposed bedrock (F_e) decreases.

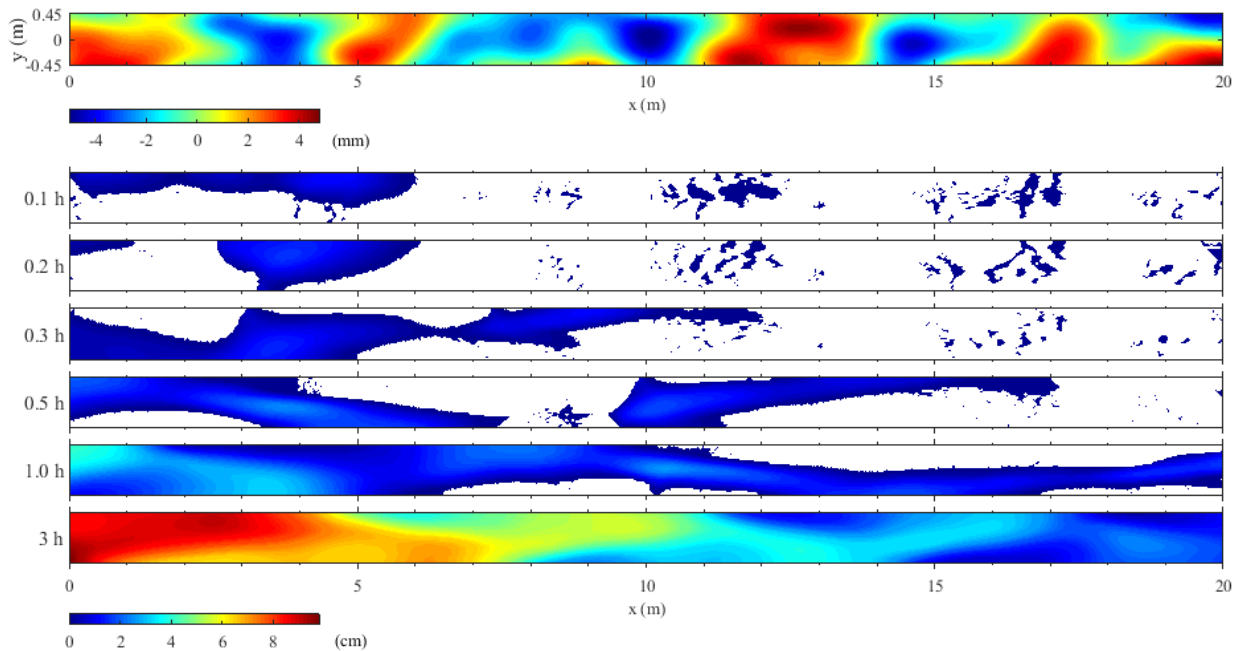


Figure 1. Plan view of bedrock topography (top). Colorbar scale indicates the detrended bed elevation. Simulated bed evolution of Run 2-Bx with $q_s/q_c = 1$ (bottom). Colorbar shows the thickness of the sediment cover, and white areas correspond to the exposed bedrock surface.

261 Figure 3 shows the time evolution of alluvial patch formation for simulation Run 2-Bx,
 262 which commenced from the bare bedrock bed in a channel with a higher slope of 0.02. For this
 263 run, bedrock roughness was 4 mm and sediment was supplied at the channel's transport capacity
 264 ($q_s/q_c = 1$). The sediment tends to deposit on the stoss side of the bedrock mounds where low
 265 flow velocity results in low Froude number, shear stress, and sediment transport capacity. The
 266 sediment forms small patches that grow in size as they move downstream. The migrating alluvial
 267 patches bypass the high bedrock areas by moving through the topographic lows. A sediment strip
 268 develops and shifts from one side of the channel to the other, and the entire channel bed is
 269 eventually covered with sediment. Complete alluviation of the bedrock bed begins from the
 270 upstream end of the channel, and alternate-bar-like patterns form as sediment moves across the
 271 channel.

272 Unlike the lower-slope runs of 2-Dx, simulations for 2-Ax ($S = 0.0115$) and 2-Bx ($S = 0.02$)
 273 were not able to achieve persistent alluvial cover for sediment supplies less than the
 274 transport capacity. Figure 4a demonstrates how the fraction of exposed bedrock surface varies
 275 with the sediment supply to transport capacity ratio in the initially bare bedrock channel. In
 276 steep-slope channels ($S \geq 0.0115$) without preexisting sediment, the bedrock bed remains fully

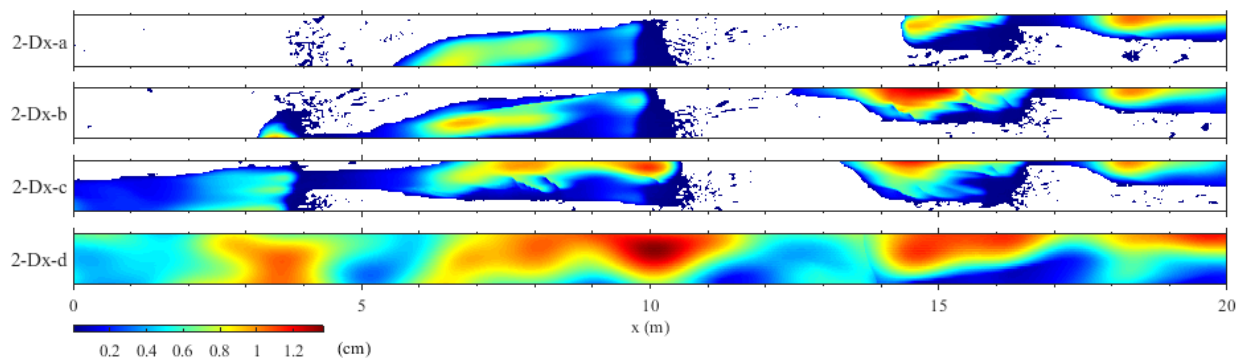


Figure 3. Plan view of Runs 2-Dx at equilibrium. The sediment is supplied at $q_s/q_c = 0.25, 0.5, 0.75,$ and 1.0 , from top to bottom. Colorbar shows the thickness of the sediment cover, and white areas correspond to the exposed bedrock surface.

277 exposed while the sediment supply rate is less than the channel sediment transport capacity.
 278 When the sediment supply momentarily exceeds the threshold value, the entire bedrock bed is
 279 completely covered by sediment, so-called “runaway alluviation”. In contrast, in the lower slope
 280 channel ($S = 0.003$, Run 2-Dx), the fractional bedrock exposure declines with increasing
 281 sediment supply in a more or less linear fashion at below-capacity sediment supply. These results
 282 are qualitatively and quantitatively similar to the observations of Chatanantavet and Parker
 283 (2008), whose experimental results are plotted alongside ours on the same figure (Figure 4).

284 3.2 Simulations with initial alluvial cover and varying slope

285 Figure 4b compares the model-predicted and experimentally observed relationships
 286 between bedrock exposure fraction and sediment supply in channels with initial sediment cover.
 287 In a steeper slope channel ($S = 0.02$, Run 2-B), the bedrock is completely exposed when the
 288 sediment supply to transport capacity rate is less than 0.4. However, a linear relationship
 289 between the extent of sediment cover and sediment supply is exhibited when the sediment supply
 290 exceeds the threshold value ($q_s/q_c > 0.6$). This threshold sediment supply rate beyond which
 291 there is a linear relationship between sediment cover fraction and sediment supply ratio

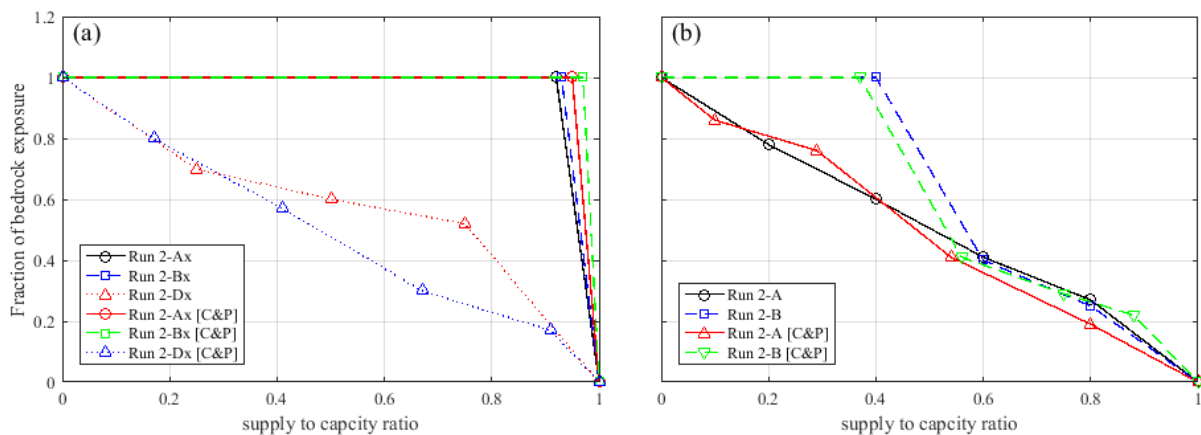


Figure 4. Results from the numerical simulations and flume experiments (Chatanantavet & Parker, 2008) of the fraction of bedrock exposure with varying sediment supply to transport capacity ratio for the simulations commenced from (a) bare bedrock channel and (b) alluvial channel.

292 decreases as the channel slope decreases (Run 2-A). In a channel slope of 0.0115, the linear
 293 relationship is observed throughout the entire range of q_s/q_c that the fraction of bedrock
 294 exposure increases gradually as the sediment supply to capacity ratio decreases.

295 3.3 Simulations with various initial sediment layer thickness

296 The simulations of Runs 2-B2 and 2-B2-a to 2-B2-c are conducted to explore the effect
 297 of antecedent sediment layer thickness on alluvial patterns. Figure 5 shows the time evolution of
 298 bedrock exposure and averaged alluvial thickness in the 2 % slope channel for both the
 299 simulations and Chatanantavet and Parker (2008) experiments. The initial sediment cover
 300 thickness was varied between 1 and 6 cm while the sediment flux of 66 g/s is constantly
 301 supplied. In the simulation starting with 1 cm sediment cover thickness, the sediment quickly
 302 erodes and washes out from the channel. The simulations with 2 cm or higher initial alluvial
 303 thickness present that the fraction of bedrock exposure increases gradually and converges
 304 approximately at 0.4. For those runs, the mean alluvial layer thickness over the sediment-covered
 305 area evolves toward 2 cm when the initial cover thickness equals or exceeds 2 cm.

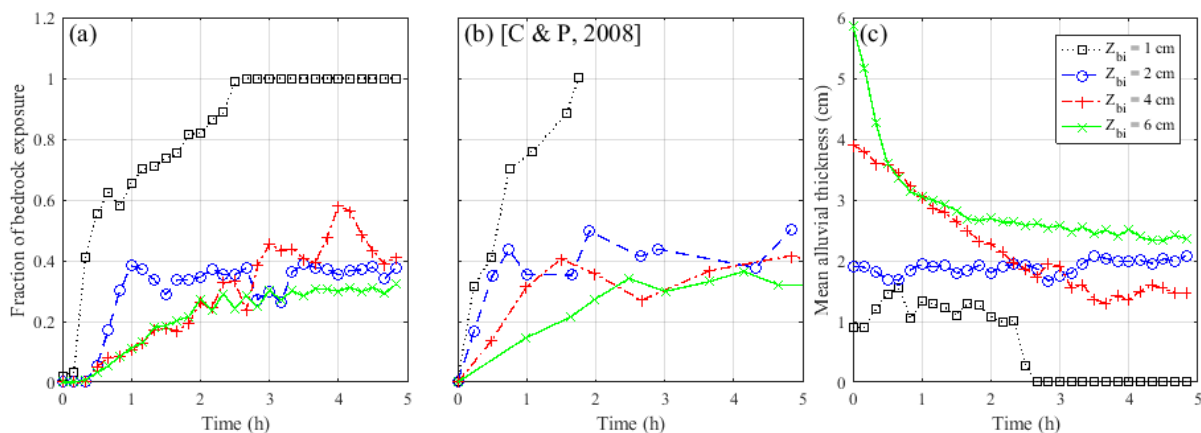


Figure 5. The time evolution of the (a) fraction of bedrock exposure from numerical simulations, (b) flume experiments (Chatanantavet & Parker, 2008), and (c) alluvial cover thickness averaged over the covered area only. The Runs of 2-B2-a, 2-B2, 2-B2-b, and 2-B2-c correspond to the initial cover thickness of 1, 2, 4, and 6 cm, respectively.

306 **4 Discussion**

307 Our results replicated several phenomena observed in the Chatanantavet & Parker (2008)
308 experiments: 1) runaway alluviation for high-slope channels with no initial sediment cover, and
309 gradual alluviation for low-slope channels with no initial sediment cover (Figure 4a), 2) a
310 threshold sediment supply for higher-slope channels with the initial cover below which sediment
311 washes out, but above which a linear relationship between sediment supply and fraction exposure
312 develops (Figure 4b), and 3) a threshold initial sediment cover thickness above which quasi-
313 steady sediment cover develops, but below which full bedrock exposure and sediment washout
314 occurs. The model's complete description of the hydrodynamic and sediment transport
315 conditions throughout the experiments help explain why these phenomena occurred.

316 4.1 Runaway alluviation vs. gradual alluviation

317 The gradual decrease in the fraction of bedrock exposed with increasing sediment supply
318 at the low-slope (2-Dx) condition, and the runaway alluviation at higher slopes where persistent
319 (total) sediment cover occurred only at sediment supply greater than the transport capacity, with
320 complete bedrock exposure at sediment supplies below that value, was observed in both our
321 numerical simulations and in the experiments of Chatanantavet and Parker (2008). Chatanantavet
322 and Parker (2008) suggested that this phenomenon may be in part due to sediment grain
323 interactions, such that at low slopes, frequent grain collisions lead to the development of alluvial
324 patches, which then increase local roughness and grow in size, whereas at higher slopes those
325 collisions may be less frequent and less likely to develop incipient patches. Hodge and Hoey's
326 (2012) cellular automata model runs with varying grain entrainment probability on bedrock and
327 alluvial surfaces suggest that the much higher grain entrainment probability on the bedrock
328 surface than the alluvial surface is a key factor of runaway alluviation.

329 Our model treats sediment transport as a continuum and is therefore not able to model
 330 grain interactions directly, but it still exhibited the same sort of slope-dependent relationship
 331 between gradual vs. runaway alluviation. Our model results suggest this is a result of the
 332 development of transcritical flows over bare low-slope beds, but not in higher-slope channels.

333 Figure 6 shows the Froude numbers calculated in the bare bedrock channel before
 334 feeding sediment at the inlet for the Runs 2-Ax, 2-Bx, and 2-Dx. The flow is supercritical in
 335 steep slope channels (2-Ax and 2-Bx), while locally subcritical flow is observed in lower slope
 336 channels (2-Dx). The flow field variables and shear stress result in a low sediment transport
 337 capacity where the flow is subcritical in the low-slope channel (Figure 7). These subcritical
 338 zones become areas of deposition, inducing a cascade of local changes in roughness, velocity,
 339 shear stress, and critical dimensionless shear stress which permit the growth of alluvial patches.
 340 However, in the steep slope channels, the large sediment transport capacity produced by high
 341 flow velocity and shear stress results in the particles passing through the channel reach without
 342 ever residing on the bed when the sediment supply is less than the transport capacity (Figure 4a).

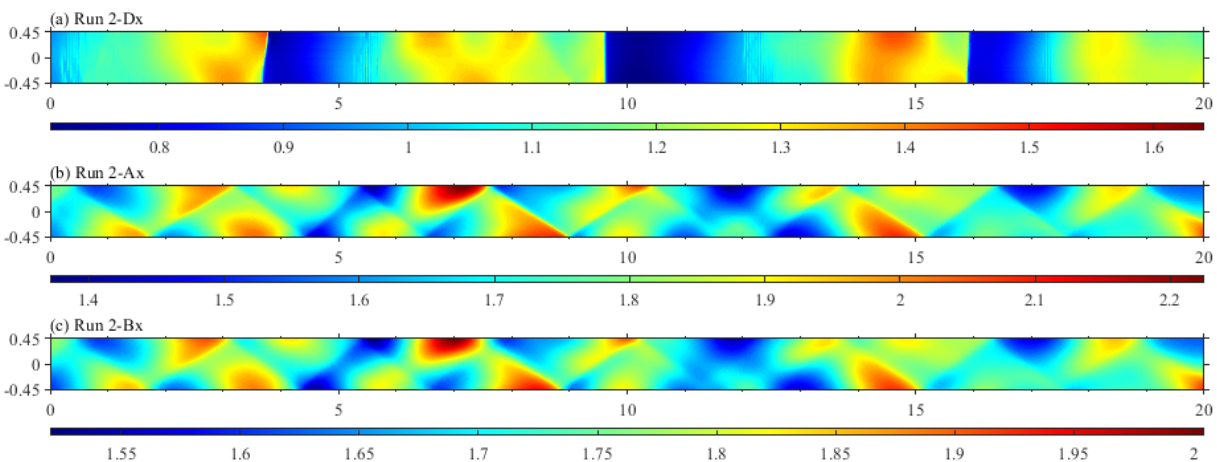


Figure 6. Initially calculated Froude number for Runs (a) 2-Dx, (b) 2-Ax, and (c) 2-Bx in bare bedrock channel. Colorbars indicate the scale of computed values, respectively.

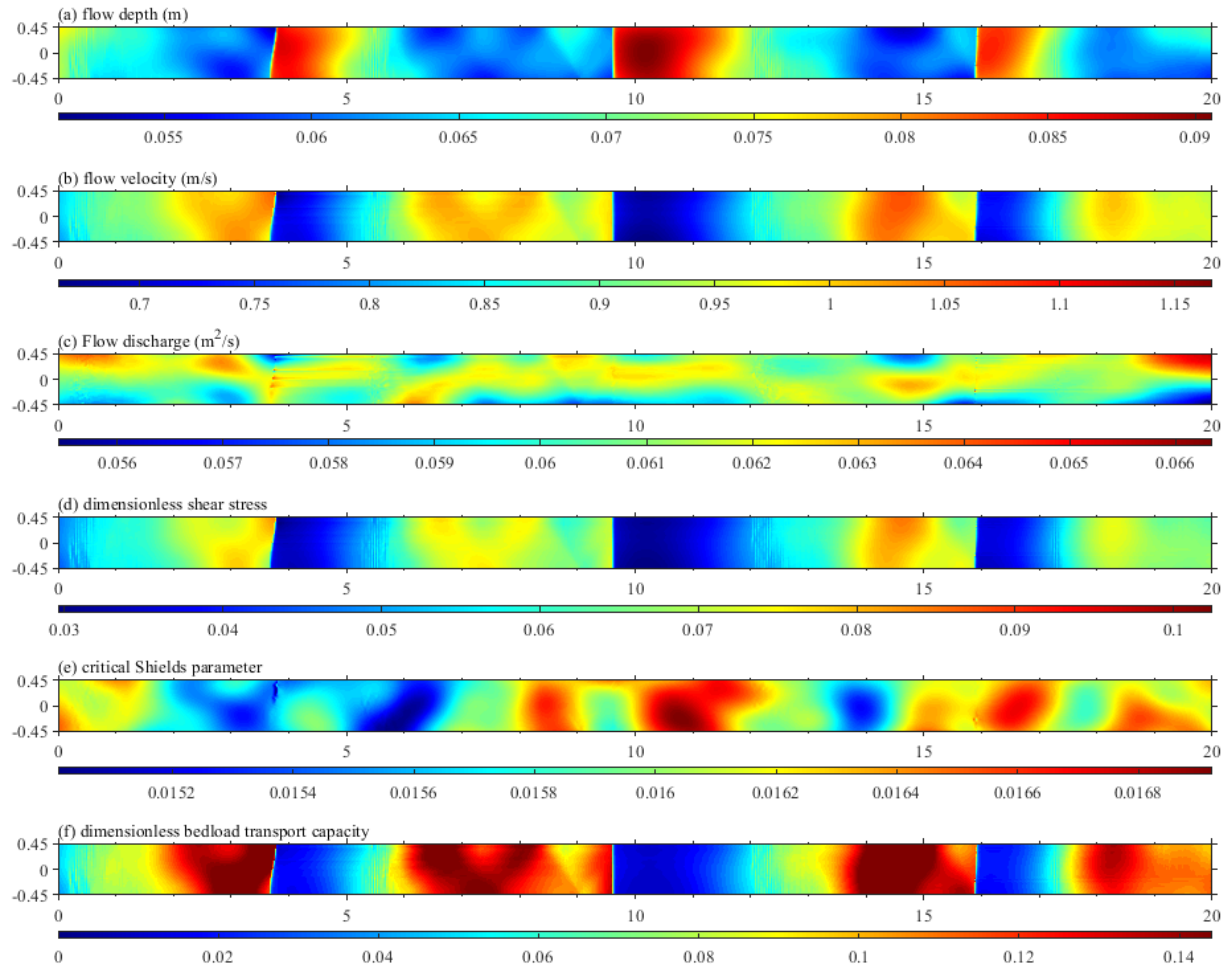


Figure 7. Initially calculated variables in bare bedrock channel for the Run 2-Dx: (a) flow depth, (b) flow velocity, (c) flow discharge, (d) dimensionless shear stress, (e) critical Shields parameter, and (f) dimensionless bedload transport capacity. Colorbars indicate the scale of computed values, respectively.

343 Thus, while grain interactions and roughness feedbacks may play a role in developing
 344 persistent alluvial sediment cover at below-capacity sediment supply in low-slope channels, the
 345 flow field – especially the presence of regions of transcritical flow – may be a necessary and
 346 important condition leading to this behavior.

347 4.2 Sediment supply threshold for persistent alluvial patches

348 The 2 % slope channel simulations with 2 cm initial cover thickness (Runs 2-B1, 2-B2, 2-
 349 B3, and 2-B4) show sediment washing out when the sediment supply rate is less than the

350 threshold capacity of about . The sediment forms alternate bars that produce additional
 351 resistance to the flow. The increased form drag roughness competes with decreased bed surface
 352 roughness due to exposed bedrock beds. The channel experiences complete bedrock exposure
 353 when the sediment supply does not meet the threshold amount to maintain the bedform. In other
 354 words, the sediment supplied to the system is redistributed to create bedforms which increase
 355 overall roughness and encourage sediment deposition and persistence of the alluvial cover; if the
 356 supply is insufficient to build the bedforms, the overall roughness decreases as bedrock becomes
 357 exposed and all of the sediment washes out (Figure 8).

358 Similar mechanisms explain the relationship between the initial thickness of sediment
 359 cover and the development of persistent alluvial cover as opposed to sediment washout at below-
 360 threshold initial thicknesses (Figure 5). The 1.15 % slope channel simulations with 1.5 cm initial
 361 cover thickness (Runs 2-A1 through 2-A5) show the linear relationship between the fraction
 362 cover and sediment supply to transport capacity. Transcritical flow is observed in this simulation
 363 (Figure 9). The flow is subcritical in the alluvial area and supercritical over the bedrock surface.
 364 The sediment forms a series of discrete sediment patches with a thin layer rather than a

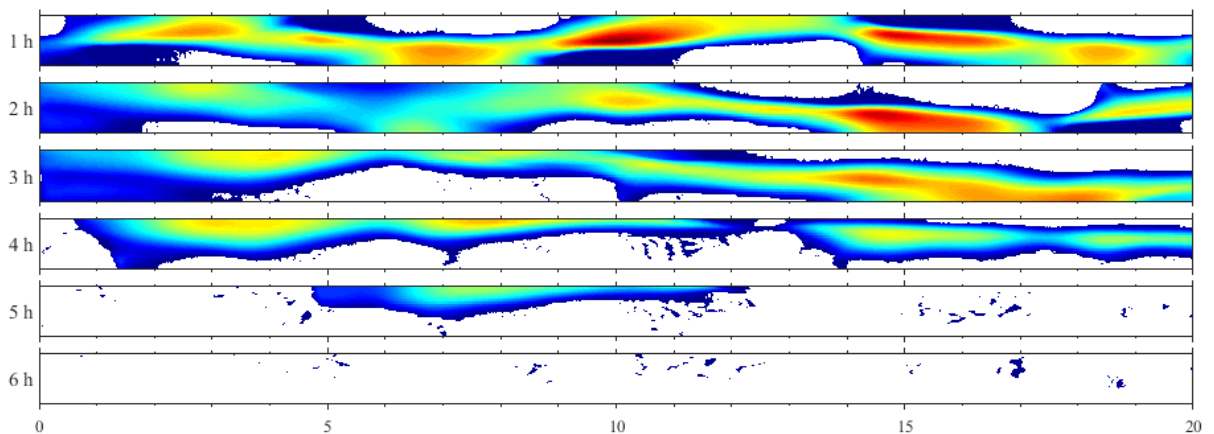


Figure 8. Simulated bed evolution of Run 2-B1 with $q_s/q_c = 0.4$. Colorbar shows the thickness of the sediment cover, and white areas correspond to the exposed bedrock surface.

365 continuous strip of sediment. The subcritical flow promotes the thin layer of alluvial patches to
 366 form even in low sediment supply channels.

367 Figure 10 shows how roughness changes from the initial value of grain and sediment
 368 transport roughness, form drag, and total hydraulic roughness through time. The non-bedform

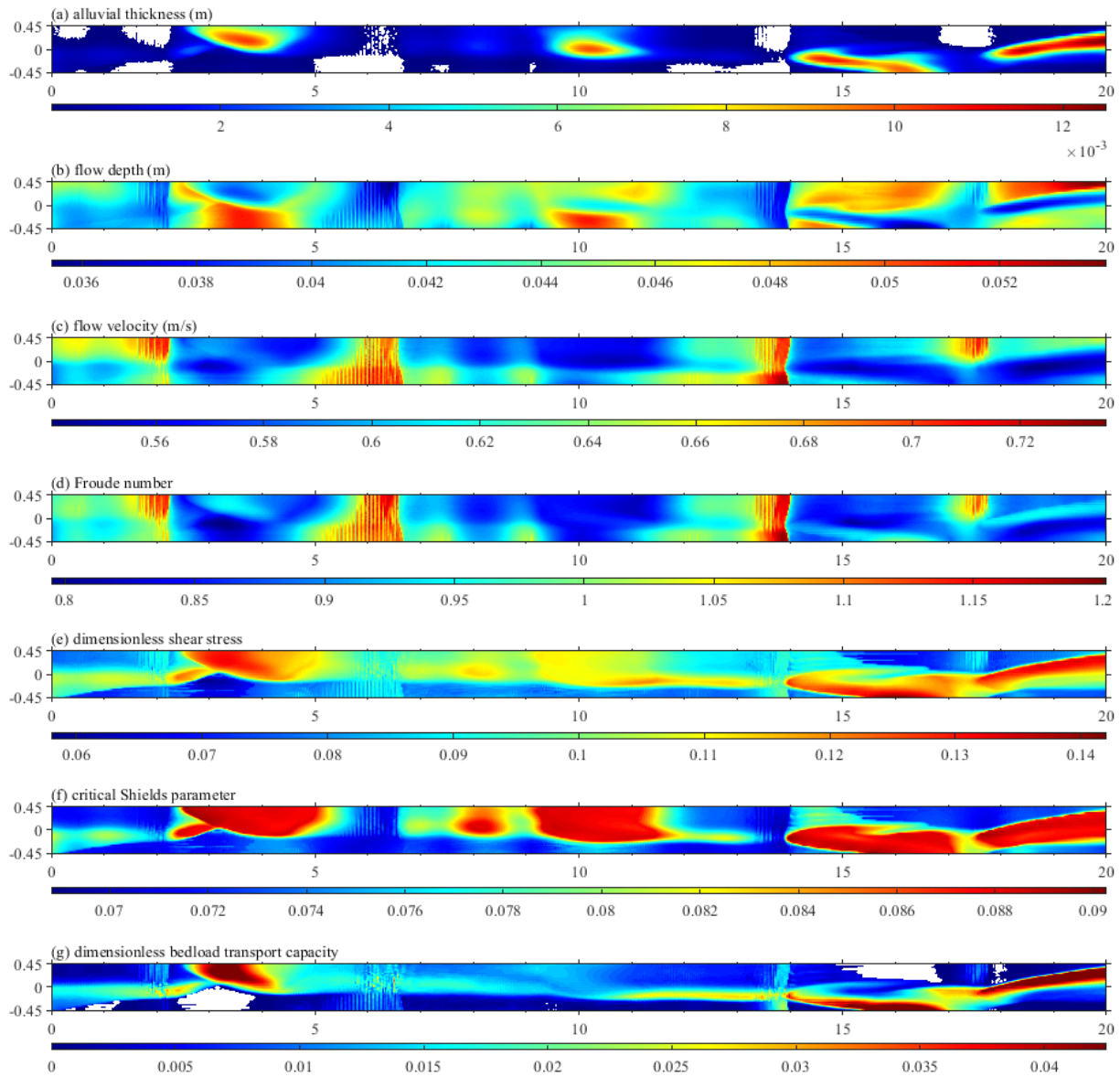


Figure 9. Simulation results commenced from alluvial channel for the Run 2-A2 at $t = 5$ h: (a) alluvial thickness, (b) flow depth, (c) flow velocity, (d) Froude number, (e) dimensionless shear stress, (f) critical Shields parameter, and (g) dimensionless bedload transport capacity. Colorbars indicate the scale of computed values, respectively. White areas correspond to (a) the exposed bedrock surface and (g) no bedload transport.

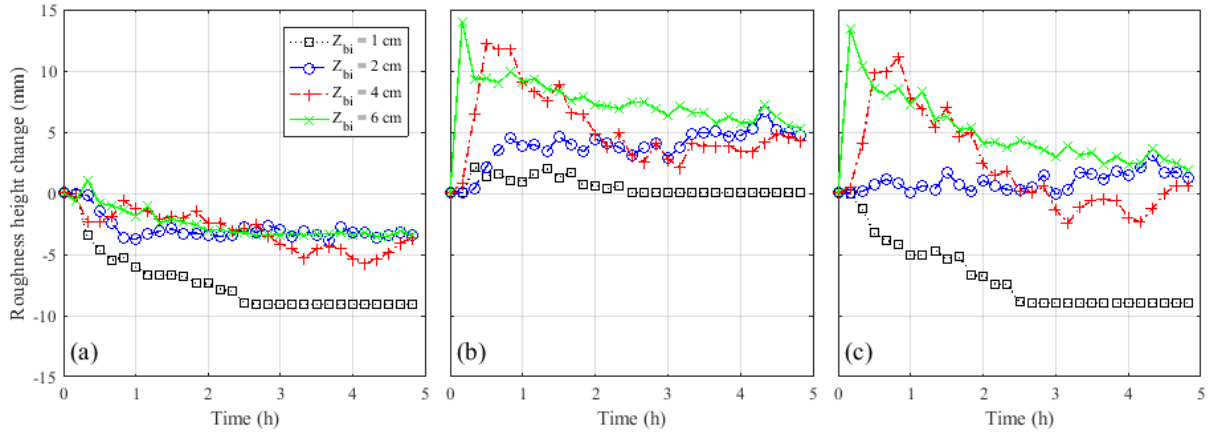


Figure 10. The time evolution of roughness difference from the initial roughness value: (a) bed surface roughness, (b) bedform roughness, and (c) total hydraulic roughness. The Runs of 2-B2-a, 2-B2, 2-B2-b, and 2-B2-c correspond to the initial cover thickness of 1, 2, 4, and 6 cm, respectively.

369 roughness gradually decreases as bedrock exposure increases for all Runs of 2-B2. However, the
 370 bedform roughness of Runs 2-B2, 2-B2-b, and 2-B2-c increases to 5 mm at the equilibrium state,
 371 whereas the bedform roughness of Run 2-B2-a increases at the early stage and decreases back to
 372 0. The changes in total roughness height indicate that the channel initially requires a thicker
 373 sediment cover layer than the threshold value to develop bars and maintain alluvial strips, or
 374 sediment washing out occurs.

375 5 Conclusions

376 We used a two-dimensional morphodynamic model to conduct a series of numerical
 377 experiments in the mixed bedrock-alluvial channel. This study explores the interaction between
 378 bedrock alluviation and morphological evolution. Simulations with varying sediment supply are
 379 conducted in different slope and antecedent channel conditions. The model replicated
 380 observations from a mixed bedrock-alluvial experiment (Chatanantavet & Parker, 2008),
 381 including a) the relationship between channel slope and gradual vs. runaway alluviation, b) the
 382 slope-dependent sediment supply threshold for development of persistent alluvial cover, c) the
 383 relationship between decreasing bedrock exposure and increasing sediment supply, and d) the

384 development of constant alluvial cover thickness regardless of initial sediment thickness,
385 provided the initial thickness exceeds a minimum value necessary to maintain bedform
386 dimensions.

387 The model results provide physical insight on the mechanisms responsible for these
388 phenomena. Transcritical flow plays an important role in initiating sediment deposition over
389 initially bare bedrock, and the development of transcritical zones in low-slope simulations but
390 not high-slope simulations may explain the apparent slope dependence of runaway alluviation.
391 Persistent sediment cover in high-slope channels is possible when rough alluvial surfaces balance
392 the extent of lower-roughness bedrock surfaces, and steeper channels require higher sediment
393 supply to exceed an apparent threshold where that balance can occur.

394 **Open Research**

395 The output data from numerical simulations used in this analysis can be found at
396 <https://github.com/rcemorpho/morph2d>.

397 **References**

398 Buffington, J. M., Montgomery, D. R., & Greenberg, H. M. (2004). Basin-scale availability of
399 salmonid spawning gravel as influenced by channel type and hydraulic roughness in
400 mountain catchments. *Canadian Journal of Fisheries and Aquatic Sciences*, *61*(11),
401 2085–2096. <https://doi.org/10.1139/f04-141>

402 Calantoni, J. (2002). Discrete particle model for bedload sediment transport in the surf zone. In
403 *ProQuest Dissertations and Theses*.
404 [https://search.proquest.com/docview/305510563?accountid=6180%0Ahttp://dw2zn6fm9](https://search.proquest.com/docview/305510563?accountid=6180%0Ahttp://dw2zn6fm9z.search.serialssolution.com?ctx_ver=Z39.88-2004&ctx_enc=info:ofi/enc:UTF-)
405 [z.search.serialssolution.com?ctx_ver=Z39.88-2004&ctx_enc=info:ofi/enc:UTF-](https://search.proquest.com/docview/305510563?accountid=6180%0Ahttp://dw2zn6fm9z.search.serialssolution.com?ctx_ver=Z39.88-2004&ctx_enc=info:ofi/enc:UTF-)

- 406 8&rft_id=info:sid/ProQuest+Dissertations+%26+Theses+Global&rft_val_fmt=info:ofi/f
407 mt:kev:mtx:dissertati
- 408 Chatanantavet, P., & Parker, G. (2008). Experimental study of bedrock channel alluviation under
409 varied sediment supply and hydraulic conditions. *Water Resources Research*, 44(12), 1–
410 19. <https://doi.org/10.1029/2007WR006581>
- 411 Demeter, G. I., Sklar, L. S., & Davis, J. R. (2005). The influence of variable sediment supply and
412 bed roughness on the spatial distribution of incision in a laboratory bedrock channel.
413 *2005 Fall Meeting of the AGU*, 2004.
- 414 Detert, M., & Parker, G. (2010). Estimation of the Washout Depth of Fine Sediments from a
415 Granular Bed. *Journal of Hydraulic Engineering*, 136(10), 790–793.
416 [https://doi.org/10.1061/\(ASCE\)HY.1943-7900.0000263](https://doi.org/10.1061/(ASCE)HY.1943-7900.0000263)
- 417 Duan, J. G., & Julien, P. Y. (2005). Numerical simulation of the inception of channel
418 meandering. *Earth Surface Processes and Landforms*, 30(9), 1093–1110.
419 <https://doi.org/10.1002/esp.1264>
- 420 Finnegan, N. J., Sklar, L. S., & Fuller, T. K. (2007). Interplay of sediment supply, river incision,
421 and channel morphology revealed by the transient evolution of an experimental bedrock
422 channel. *Journal of Geophysical Research: Earth Surface*, 112(3), 1–17.
423 <https://doi.org/10.1029/2006JF000569>
- 424 Hartshorn, K., Hovius, N., Dade, W. B., & Slingerland, R. L. (2002). Climate-driven bedrock
425 incision in an active mountain belt. *Science*, 297(5589), 2036–2038.
426 <https://doi.org/10.1126/science.1075078>

- 427 Hodge, R. A., & Hoey, T. B. (2012). Upscaling from grain-scale processes to alluviation in
428 bedrock channels using a cellular automaton model. *Journal of Geophysical Research:
429 Earth Surface*, 117(F1), n/a-n/a. <https://doi.org/10.1029/2011JF002145>
- 430 Hodge, R. A., & Hoey, T. B. (2016a). A Froude-scaled model of a bedrock-alluvial channel
431 reach: 1. Hydraulics. *Journal of Geophysical Research: Earth Surface*, 121(9), 1578–
432 1596. <https://doi.org/10.1002/2015JF003706>
- 433 Hodge, R. A., & Hoey, T. B. (2016b). A Froude-scaled model of a bedrock-alluvial channel
434 reach: 2. Sediment cover. *Journal of Geophysical Research: Earth Surface*, 121(9),
435 1597–1618. <https://doi.org/10.1002/2015JF003709>
- 436 Howard, A. D. (1980). Thresholds in river regimes. In *Thresholds in Geomorphology* (pp. 227–
437 258).
- 438 Howard, A. D., Dietrich, W. E., & Seidl, M. A. (1994). Modeling fluvial erosion on regional to
439 continental scales. *Journal of Geophysical Research: Solid Earth*, 99(B7), 13971–13986.
440 <https://doi.org/10.1029/94JB00744>
- 441 Howard, A. D., & Kerby, G. (1983). Channel changes in badlands. *Geological Society of
442 America Bulletin*, 94(6), 739. [https://doi.org/10.1130/0016-
443 7606\(1983\)94<739:CCIB>2.0.CO;2](https://doi.org/10.1130/0016-7606(1983)94<739:CCIB>2.0.CO;2)
- 444 Huston, D. L., & Fox, J. F. (2015). Clogging of Fine Sediment within Gravel Substrates:
445 Dimensional Analysis and Macroanalysis of Experiments in Hydraulic Flumes. *Journal
446 of Hydraulic Engineering*, 141(8), 1–14. [https://doi.org/10.1061/\(ASCE\)HY.1943-
447 7900.0001015](https://doi.org/10.1061/(ASCE)HY.1943-7900.0001015)

- 448 Huston, D. L., & Fox, J. F. (2016). Momentum-Impulse Model of Fine Sand Clogging Depth in
449 Gravel Streambeds for Turbulent Open-Channel Flow. *Journal of Hydraulic*
450 *Engineering*, 142(2). [https://doi.org/10.1061/\(ASCE\)HY.1943-7900.0001092](https://doi.org/10.1061/(ASCE)HY.1943-7900.0001092)
- 451 Inoue, T., Iwasaki, T., Parker, G., Shimizu, Y., Izumi, N., Stark, C. P., & Funaki, J. (2016).
452 Numerical Simulation of Effects of Sediment Supply on Bedrock Channel Morphology.
453 *Journal of Hydraulic Engineering*, 04016014. [https://doi.org/10.1061/\(ASCE\)HY.1943-](https://doi.org/10.1061/(ASCE)HY.1943-7900.0001124)
454 [7900.0001124](https://doi.org/10.1061/(ASCE)HY.1943-7900.0001124)
- 455 Inoue, T., Izumi, N., Shimizu, Y., & Parker, G. (2014). Interaction among alluvial cover, bed
456 roughness, and incision rate in purely bedrock and alluvial-bedrock channel. *Journal of*
457 *Geophysical Research: Earth Surface*, 119(10), 2123–2146.
458 <https://doi.org/10.1002/2014JF003133>
- 459 Johnson, J. P. L. (2014). A surface roughness model for predicting alluvial cover and bed load
460 transport rate in bedrock channels. *Journal of Geophysical Research: Earth Surface*,
461 *119Johnson*(10), 2147–2173. <https://doi.org/10.1002/2013JF003000>
- 462 Johnson, J. P. L., & Whipple, K. X. (2007). Feedbacks between erosion and sediment transport
463 in experimental bedrock channels. *Earth Surface Processes and Landforms*, 32(7), 1048–
464 1062. <https://doi.org/10.1002/esp.1471>
- 465 Johnson, J. P. L., & Whipple, K. X. (2010). Evaluating the controls of shear stress, sediment
466 supply, alluvial cover, and channel morphology on experimental bedrock incision rate. *J.*
467 *Geophys. Res.*, 115, F02018. <https://doi.org/10.1029/2009JF001335>
- 468 Kuhnle, R. A., Wren, D. G., Langendoen, E. J., & Rigby, J. R. (2013). Sand transport over an
469 immobile gravel substrate. *Journal of Hydraulic Engineering*, 139(2), 167–176.
470 [https://doi.org/10.1061/\(ASCE\)HY.1943-7900.0000615](https://doi.org/10.1061/(ASCE)HY.1943-7900.0000615)

- 471 Lamb, M. P., Dietrich, W. E., & Venditti, J. G. (2008). Is the critical shields stress for incipient
472 sediment motion dependent on channel-bed slope? *Journal of Geophysical Research:*
473 *Earth Surface*, 113(2), 1–20. <https://doi.org/10.1029/2007JF000831>
- 474 Lamb, M. P., Finnegan, N. J., Scheingross, J. S., & Sklar, L. S. (2015). New insights into the
475 mechanics of fluvial bedrock erosion through flume experiments and theory.
476 *Geomorphology*, 244, 33–55. <https://doi.org/10.1016/j.geomorph.2015.03.003>
- 477 Lisle, T. E., & Hilton, S. (1992). The Volume Of Fine Sediment In Pools: An Index Of Sediment
478 Supply In Gravel-Bed Streams. *Journal of the American Water Resources Association*,
479 28(2), 371–383. <https://doi.org/10.1111/j.1752-1688.1992.tb04003.x>
- 480 Lisle, T. E., & Lewis, J. (1992). Effects of Sediment Transport on Survival of Salmonid Embryos
481 in a Natural Stream: A Simulation Approach. *Canadian Journal of Fisheries and Aquatic*
482 *Sciences*, 49(11), 2337–2344. <https://doi.org/10.1139/f92-257>
- 483 Luu, L. X., Egashira, S., & Takebayashi, H. (2004). Investigation of Tan Chau Reach In Lower
484 Mekong Using Field Data And Numerical Simulation. *PROCEEDINGS OF*
485 *HYDRAULIC ENGINEERING*, 48(5), 1057–1062. <https://doi.org/10.2208/prohe.48.1057>
- 486 Madej, M. A. (2001). Development of channel organization and roughness following sediment
487 pulses in single-thread, gravel bed rivers. *Water Resources Research*, 37(8), 2259–2272.
488 <https://doi.org/10.1029/2001WR000229>
- 489 Massong, T. M., & Montgomery, D. R. (2000). Influence of sediment supply, lithology, and
490 wood debris on the distribution of bedrock and alluvial channels. *Geological Society of*
491 *America Bulletin*, 112(4), 591–599. [https://doi.org/10.1130/0016-](https://doi.org/10.1130/0016-7606(2000)112<591:IOSSLA>2.0.CO;2)
492 [7606\(2000\)112<591:IOSSLA>2.0.CO;2](https://doi.org/10.1130/0016-7606(2000)112<591:IOSSLA>2.0.CO;2)

- 493 McLean, S. R., Nelson, J. M., & Wolfe, S. R. (1994). Turbulence structure over two-dimensional
494 bed forms: Implications for sediment transport. *Journal of Geophysical Research*,
495 99(C6), 12729. <https://doi.org/10.1029/94JC00571>
- 496 Mishra, J., & Inoue, T. (2020). Alluvial cover on bedrock channels: applicability of existing
497 models. *Earth Surface Dynamics*, 8(3), 695–716. [https://doi.org/10.5194/esurf-8-695-](https://doi.org/10.5194/esurf-8-695-2020)
498 2020
- 499 Montgomery, D. R., Abbe, T. B., Buffington, J. M., Peterson, N. P., Schmidt, K. M., & Stock, J.
500 D. (1996). Distribution of bedrock and alluvial channels in forested mountain drainage
501 basins. In *Nature* (Vol. 381, Issue 6583, pp. 587–589). <https://doi.org/10.1038/381587a0>
- 502 Montgomery, D. R., & Buffington, J. M. (1997). Channel-reach morphology in mountain
503 drainage basins. *Bulletin of the Geological Society of America*, 109(5), 596–611.
504 [https://doi.org/10.1130/0016-7606\(1997\)109<0596:CRMIMD>2.3.CO](https://doi.org/10.1130/0016-7606(1997)109<0596:CRMIMD>2.3.CO)
- 505 Nelson, J. M., Bennett, J. P., & Wiele, S. M. (2003). Flow and sediment-transport modeling.
506 *Tools in Fluvial Geomorphology*. <https://doi.org/10.1002/0470868333.ch18>
- 507 Ribberink, J. S. (1987). Mathematical modelling of one-dimensional morphological changes in
508 rivers with non-uniform sediment. *Communications on Hydraulic & Geotechnical*
509 *Engineering - Delft University of Technology*, 87–2.
- 510 Sklar, L., & Dietrich, W. (1998). River longitudinal profiles and bedrock incision models:
511 Stream power and the influence of sediment supply. In K. J. Tinkler & E. E. Wohl (Eds.),
512 *Rivers Over Rock: Fluvial Processes in Bedrock Channels* (Volume 107, pp. 237–260).
513 <https://doi.org/10.1029/GM107p0237>

- 514 Sklar, L., & Dietrich, W. (2001). Sediment and rock strength controls on river incision into
515 bedrock. *Geology*, 29(12), 1087. [https://doi.org/10.1130/0091-](https://doi.org/10.1130/0091-7613(2001)029<1087:SARSCO>2.0.CO;2)
516 [7613\(2001\)029<1087:SARSCO>2.0.CO;2](https://doi.org/10.1130/0091-7613(2001)029<1087:SARSCO>2.0.CO;2)
- 517 Sklar, L., & Dietrich, W. (2004). A mechanistic model for river incision into bedrock by
518 saltating bed load. *Water Resources Research*, 40(6), 1–21.
519 <https://doi.org/10.1029/2003WR002496>
- 520 Soulsby, R. (1997). Dynamics of Marine Sands. In *Dynamics of Marine Sands*. Thomas Telford
521 Ltd. <https://doi.org/10.1680/DOMS.25844>
- 522 Struiksma, N. (1985). Prediction of 2-D bed topography in rivers. *Journal of Hydraulic*
523 *Engineering*, 111(8), 1169–1182. [https://doi.org/10.1061/\(ASCE\)0733-](https://doi.org/10.1061/(ASCE)0733-9429(1985)111:8(1169))
524 [9429\(1985\)111:8\(1169\)](https://doi.org/10.1061/(ASCE)0733-9429(1985)111:8(1169))
- 525 Talmon, A. M., Struiksma, N., & Van Mierlo, M. C. L. M. (1995). Laboratory measurements of
526 the direction of sediment transport on transverse alluvial-bed slopes. *Journal of*
527 *Hydraulic Research*, 33(4), 495–517. <https://doi.org/10.1080/00221689509498657>
- 528 Toro, E. F. (1992a). The weighted average flux method applied to the Euler equations.
529 *Philosophical Transactions of the Royal Society of London. Series A: Physical and*
530 *Engineering Sciences*, 341(1662), 499–530. <https://doi.org/10.1098/rsta.1992.0113>
- 531 Toro, E. F. (1992b). Riemann Problems and the WAF Method for Solving the Two-Dimensional
532 Shallow Water Equations. *Philosophical Transactions of the Royal Society A:*
533 *Mathematical, Physical and Engineering Sciences*, 338(1649), 43–68.
534 <https://doi.org/10.1098/rsta.1992.0002>
- 535 Tubino, M., Repetto, R., & Zolezzi, G. (1999). Free bars in rivers. *Journal of Hydraulic*
536 *Research*, 37(6), 759–775. <https://doi.org/10.1080/00221689909498510>

- 537 Turowski, J. M., Hovius, N., Meng-Long, H., Lague, D., & Men-Chiang, C. (2008). Distribution
538 of erosion across bedrock channels. *Earth Surface Processes and Landforms*, 33(3), 353–
539 363. <https://doi.org/10.1002/esp.1559>
- 540 Turowski, J. M., Hovius, N., Wilson, A., & Horng, M. J. (2008). Hydraulic geometry, river
541 sediment and the definition of bedrock channels. *Geomorphology*, 99(1–4), 26–38.
542 <https://doi.org/10.1016/j.geomorph.2007.10.001>
- 543 Turowski, J. M., Lague, D., & Hovius, N. (2007). Cover effect in bedrock abrasion: A new
544 derivation and its implications for the modeling of bedrock channel morphology. *Journal*
545 *of Geophysical Research: Earth Surface*, 112(4), 1–16.
546 <https://doi.org/10.1029/2006JF000697>
- 547 Vermeer, K. (1986). The ripple factor in sediment transport equations. *Rep. R657/M1314-V*.
- 548 Wong, M., Parker, G., DeVries, P., Brown, T. M., & Burges, S. J. (2007). Experiments on
549 dispersion of tracer stones under lower-regime plane-bed equilibrium bed load transport.
550 *Water Resources Research*, 43(3), n/a-n/a. <https://doi.org/10.1029/2006WR005172>
- 551 Zhang, L., Parker, G., Stark, C., Inoue, T., Viparelli, E., Fu, X., & Izumi, N. (2015). Macro-
552 roughness model of bedrock-alluvial river morphodynamics. *Earth Surface Dynamics*,
553 3(1), 113–138. <https://doi.org/10.5194/esurf-3-113-2015>